Pergamon

Int. J. Solids Structures Vol. 33, No. 18, pp. 2543–2574, 1996
Published by Elsevier Science Ltd

0020–7683/96 $15.00 + .00

0020–7683(95)00172–7

COMPARISON OF SHEAR-LAG THEORY AND CONTINUUM FRACTURE MECHANICS FOR MODELING FIBER AND MATRIX STRESSES IN AN ELASTIC CRACKED COMPOSITE LAMINA

IRENE J. BEYERLEIN, S. LEIGH PHOENIX
Department of Theoretical and Applied Mechanics, Cornell University, Ithaca, NY 14853, U.S.A.

and

ANN MARIE SASTRY†
Sandia National Laboratories, Albuquerque, NM 87111, U.S.A.

(*Received* 20 *March* 1995; *in revised form* 12 *July* 1995)

Abstract—This study analyzes fiber tensile and matrix shear stresses near the crack tip in a transversely cracked, unidirectional, fiber-reinforced lamina under a remote tensile stress applied in the fiber direction. The two-dimensional lamina consists of parallel, equally-spaced elastic fibers with elastic matrix in-between, and contains a row of up to a few hundred contiguous fiber breaks aligned transverse to the fiber direction forming a central transverse crack. Using the break-influence superposition (BIS) technique, a recently developed method for analyzing a shear-lag model first introduced by Hedgepeth, we calculate the tensile and shear stress concentrations in the fibers and matrix, respectively. These are compared to tensile and shear stresses calculated using Linear Elastic Fracture Mechanics (LEFM) and the complete elasticity solution both for the continuum limit of a homogeneous, orthotropic elastic material with a transverse central crack loaded in Mode I. For the shear-lag model a critical scaling parameter for examining the stress behavior away from the crack tip along the fiber direction is $\sqrt{E^*/G^*}$, where E^* and G^* are composite in-plane stiffness constants along the fiber direction and in shear, respectively. In addition to these parameters, the LEFM and complete elasticity solutions also involve the effective transverse stiffness and Poisson's ratio. For a sizable crack (consisting of 100 or more fiber breaks), the fiber tensile stresses ahead of the crack tip along the crack plane calculated from the BIS approach achieve excellent agreement with the LEFM solution down to the scale of one fiber diameter and even better agreement with the complete solution both in the near crack tip field and far field, regardless of the composite stiffness constants. The profiles of the fiber tensile and matrix shear stresses along the fiber direction show generally good agreement, with the agreement improving as the composite stiffness transverse to the fiber direction grows. Published by Elsevier Science Ltd.

1. INTRODUCTION

Brittle fiber-reinforced lamina using, say, graphite or carbon fibers are commonly used as building blocks in advanced composites due to their high specific strength and stiffness and the availability of matrix materials in a wide range of properties. For instance, one can have a polymer matrix such as an epoxy with a stiffness two orders of magnitude lower than that of the fibers, or a metal matrix such as aluminum with a stiffness of about the same order of magnitude. Matrices can be quite brittle or they can be elastic-plastic with a wide range of yield strengths. The interface strength between the fiber and matrix can also vary, as can the residual friction after debonding. Though actual structures may consist of several layers of unidirectional or multidirectional laminae, a fundamental issue is to first understand the fracture behavior of a single lamina. This is the focus of the present work.

Under simple tension, failure in a composite lamina usually begins with random fiber breaks that develop at flaws under increasing load. Consequently failure involves a complex statistical progression of random fiber failures, local stress transfer from broken to surviving fibers through shear in the matrix, and local matrix yielding and interfacial debonding

† Present address: Department of Mechanical Engineering and Applied Mechanics, The University of Michigan, Ann Arbor, MI 48109, U.S.A.

around the fiber breaks, culminating in a crack-like structure more or less perpendicular to the fiber direction (Chou, 1992). Indeed in the region one might call the "crack tip", fibers do not break precisely along one perpendicular plane even though this may be the location of the highest stress concentration. New fiber breaks are most likely to occur at some small random distance from this plane where the fiber is both overstressed and weak. Hence, the length scale along the fiber over which it is overloaded is just as important as the magnitude of the stress concentration. Furthermore, fibers pulling out behind the crack tip may modify the stress concentration. Experimental observations on metal matrix composites reveal these various non-planar crack growth features (Jones and Goree, 1983). Of course, local details of the crack growth are likely to vary with the particular material system.

Predicting the fracture behavior of unidirectional fibrous composites has been tackled in several ways including full elasticity solutions for idealized cases, various models that build on classical shear-lag analysis, and finite element methods (Goda and Phoenix, 1994; Goree and Gross, 1980; Hedgepeth and Van Dyke, 1969; Rossettos and Shishesaz, 1987; Sastry and Phoenix, 1993), and Linear Elastic Fracture Mechanics (LEFM) as though the material were a homogeneous continuum. In the case of LEFM, questions of validity quickly arise. First, since the material is actually highly anisotropic and heterogeneous, it is unclear how to interpret such singular stress field techniques in the face of inherent local length scales such as the fiber diameter, fiber spacing, and the effective fiber load transfer length near a break. This is especially true if the number of adjacent fiber breaks forming a "crack" is quite small. Second, the matrix and fiber-matrix interface can be rather weak in shear as compared, say, to a comparable shear strength in a homogeneous metal, so that considerable yielding, debonding, and fiber pullout can occur near the crack tip. This creates uncertainty in the length scale over which LEFM calculations might be useful. Third, for an orthotropic continuum LEFM techniques are complicated and often require considerable numerical computation. If the breaks are not nicely aligned, or there are clusters of breaks whose stress fields are close enough to interact (as is often the case in practice) LEFM formulations quickly become intractable. Finally LEFM techniques are often cast in terms of energy of crack propagation, and it is not clear how to reconcile this with a "strength view" of fracture progression involving local stress transfer and fiber failure at high local fiber stresses. Nevertheless, when analyzing stresses around cracks containing hundreds of contiguous fiber breaks, the composite may reasonably be idealized as a homogeneous, anisotropic continuum with a crack tip damage zone.

At the same time, shear-lag theory as pioneered by Hedgepeth (1961) has enjoyed considerable success. In this idealized model, the elastic fibers carry only simple tension and the elastic matrix in-between the fibers deforms only in simple shear. This model has seen many variations and applications largely for planar and regular geometric arrays of fiber breaks (Goree and Gross, 1979; Hedgepeth and Van Dyke, 1967; Van Dyke and Hedgepeth, 1969; Hikami and Chou, 1990; Fukuda and Chou, 1981; Fichter, 1969). Chou (1992) gives an excellent and comprehensive summary of shear-lag analysis, which highlights results from many studies and includes several references. We revisit some results from these studies in later discussion. A major criticism of the shear-lag model is that it does not model the full field equations of linear elasticity. Nevertheless, comparison with detailed 3-D finite element calculations on a composite lamina of several fibers and with a few breaks shows that the stresses determined are a good reflection of the true stresses at least locally averaged down to a length scale of about one fiber diameter (Reedy, 1984). Reedy concluded that when assuming fully elastic behavior, both the shear-lag model and 3-D finite element analysis, based on the full elasticity equations, predict nearly the same stresses on the first intact fiber even for relatively stiff matrices and for fibers with a shear modulus not much greater than that of the matrix. On the other hand, recent exact analysis and accurate numerical calculations for one fiber break (modeled as a penny-shaped crack) in a three-dimensional composite have suggested that the shear-lag model is locally inaccurate (Nedele and Wisnom, 1994; Case and Reifsnider, 1995), a conclusion we later question. A major stumbling block in the shear-lag model has been computational, but recent dramatic improvements have occurred in the ability to handle large numbers of breaks in complicated arrays (not just planar) through the development of the break

influence superposition (BIS) technique (Sastry and Phoenix, 1993). The main advantage of the shear-lag model is that it shows promise of modeling the essential physics of complex random fiber break pattern development, including matrix plasticity, fiber/matrix debonding, and fiber pullout during crack formation and propagation in a composite. Not only can hundreds of arbitrarily located breaks be handled easily, but plasticity and debonding around fiber breaks can also be treated efficiently (Sastry, 1994; Beyerlein *et al.*, 1995). Also, the shear-lag analysis uses an order of magnitude less degrees of freedom than similar 3-D finite element analysis. Therefore, compared to finite element analyses, the shear-lag analysis can handle much larger composites with many more fiber breaks, since computation time is determined by the size of the damage and not composite volume.

We now arrive at the key question: on the one hand we have a shear-lag model that may overly idealize the equations of elasticity but allows us to calculate the important fiber and matrix stresses around arrays of fiber breaks. On the other hand we have LEFM which presumably would be useful for a transverse crack covering many hundreds of fiber breaks. To what extent do the two models give similar results for crack geometries and length scales where both would presumably apply to a composite sheet? This question is important as one may worry that as the number of adjacent fiber breaks increases in an elastic setting, shear-lag theory diverges from LEFM in predicting the fiber and matrix stresses. We will show that the agreement, in fact, improves as the "crack length" grows thus clearing away one potential obstacle to using shear-lag theory to model macroscale composite failure.

Thus we consider an infinite, planar, composite lamina whose fibers and matrix are linearly elastic. The lamina has a transverse central "crack" in the form of a long row of aligned fiber breaks, and under a remote tensile load we calculate fiber and matrix stress profiles at the scale of one to a few fiber diameters near the crack tip. In homogeneous materials, this special case of a crack in a direction normal to both the loading direction and one plane of elastic symmetry is a commonly considered problem. Before describing our framework for comparison and reporting the results from the LEFM and the BIS analysis, we begin with some theoretical background for the two approaches.

2. SHEAR-LAG ANALYSIS USING BIS

Consider a large, two-dimensional array (lamina) of parallel elastic fibers in an elastic matrix with a central group of N contiguous fiber breaks transverse to the fiber direction. The lamina is loaded in simple tension along the fiber direction (Fig. 1(a)). Hedgepeth (1961) set up and analyzed a shear-lag model for this problem, and his most quoted results are the stress concentrations on the fiber immediately adjacent to the last broken fiber. As mentioned, Hedgepeth's (1961) shear lag model assumes that the matrix transmits and deforms only in shear between the fibers, but sustains no axial load. The fibers, however, carry all the tensile load, and deform only in simple tension and compression. These assumptions simplify the analysis considerably, since the differential equilibrium equations become decoupled, and, therefore, the stresses found in any given fiber or matrix bay depend only on the fiber axial coordinate x. Moreover, they also suggest that this model is appropriate for a unidirectional fiber-matrix lamina in tension, in which the fiber extensional stiffness greatly exceeds the matrix shear modulus; however, we will later consider cases where these moduli are much closer in magnitude. Many authors have modified Hedgepeth's original shear-lag analysis by modifying the geometric arrangement of fiber breaks, by accounting for matrix yielding, matrix cracking, or debonding of the fiber-matrix interface, by allowing consideration of a matrix that can carry appreciable tensile load, and by allowing for tensile stresses transverse to the fiber direction (Goree *et al.*, 1989; Rossettos and Olia, 1993; Sastry and Phoenix, 1993; Wolla and Goree, 1987; Ochiai *et al.*, 1991). However, these improvements also greatly increase the need for numerical computation for all but a few special cases. On the other hand, Hikami and Chou (1990) revisited Hedgepeth's original elastic analysis and among other things calculated simple expressions for the in-line (crack plane) stress concentrations in surviving fibers further ahead of the row of N contiguous breaks. We refer later to these analytical results since they provide a means of checking the accuracy of our numerical algorithm based on the BIS technique. Goree

and Gross (1979, 1980) extended Hedgepeth's two-dimensional model to include the effects of various arrangements of fiber breaks as well as matrix yielding and splitting. Dharani *et al.* (1983) developed another extension of Hedgepeth's model to account for both longitudinal yielding and longitudinal fiber "damage" ahead of the crack. In this model, the damaged fibers carry only a fraction of the load of an unbroken fiber reminiscent of fiber pullout or nonplanar crack growth. Featured in these works are studies of the decay of the crack plane normal stresses away from the last surviving fiber and its connection to LEFM, which are

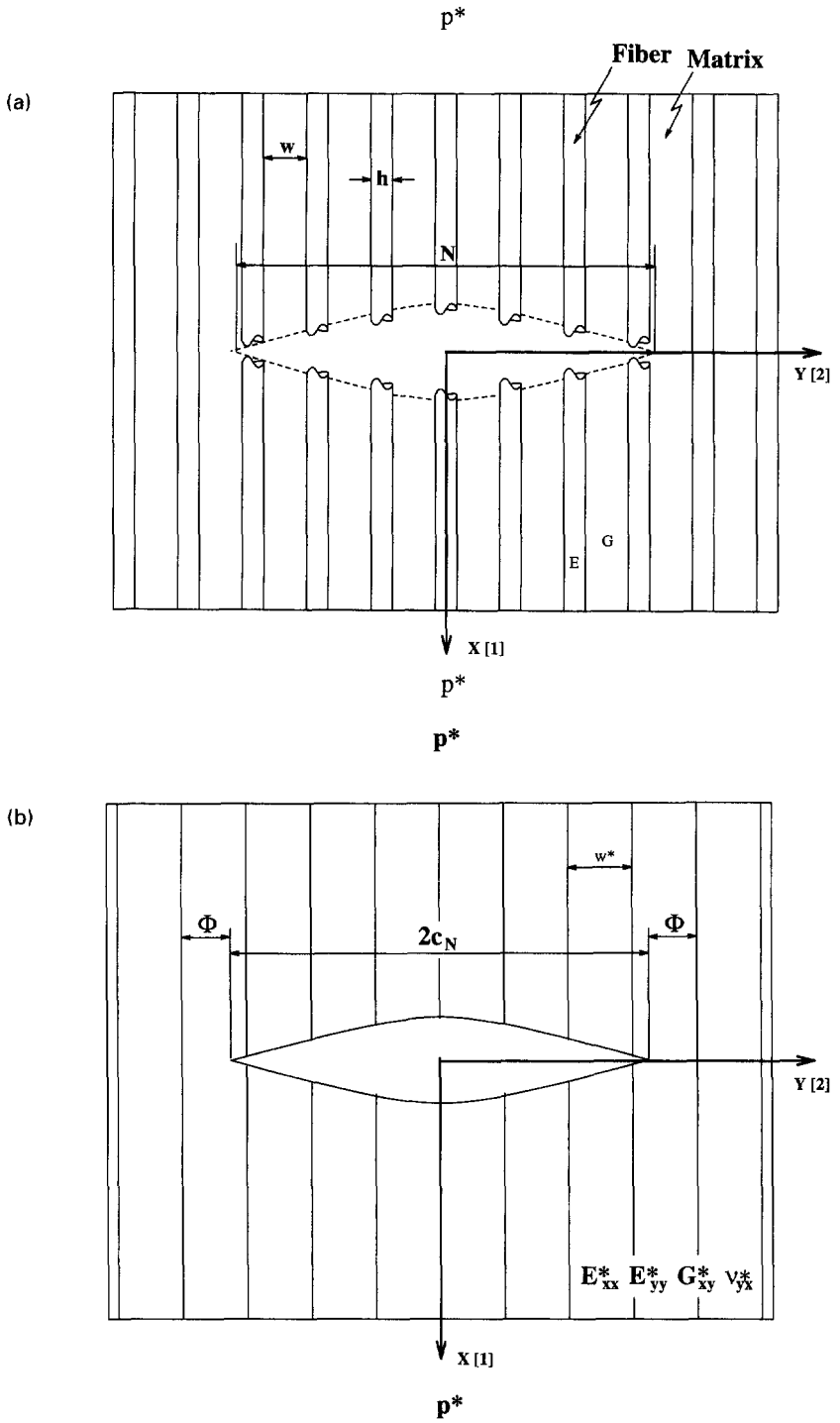

Fig. 1. Transverse center crack in three material systems: (a) fiber reinforced composite lamina, (b) a material with tension lines (corresponding to fiber centerlines) and effective matrix regions of width w^*, and (c) an orthotropic continuum. (*Continued opposite.*)

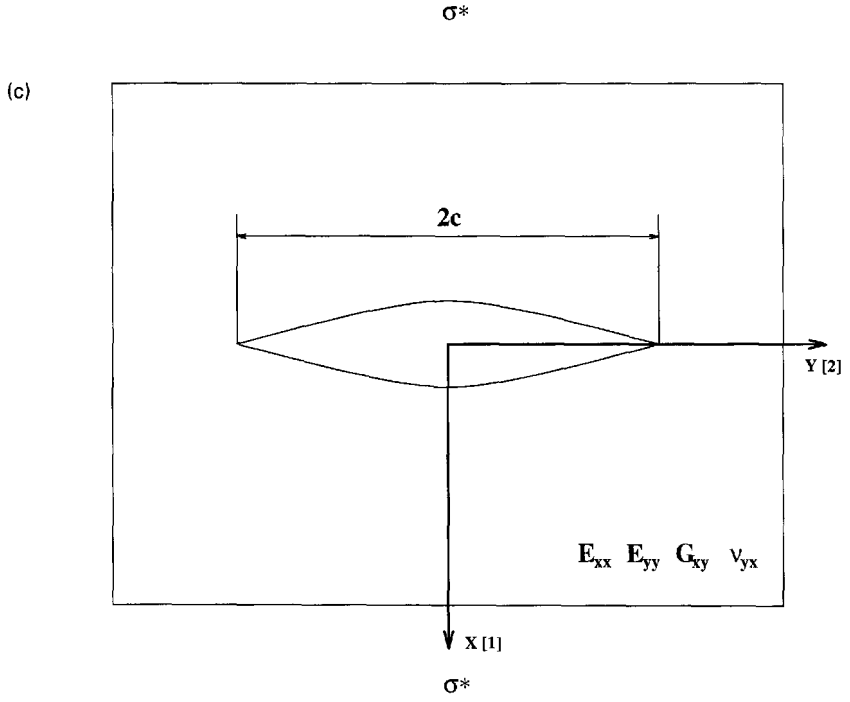

Fig. 1. *Continued.*

relevant to the present investigation. Lastly, the recently developed BIS technique (Sastry and Phoenix, 1993) extends Hedgepeth's shear-lag method to numerically determine the stress concentrations everywhere in the fiber and matrix due to arbitrarily located fiber breaks. While it has been developed to handle matrix yielding and debonding, we will use here only the simpler elastic rendition.

The simple geometry we use in carrying out the BIS technique is described in Fig. 1(a). This central transverse configuration of N aligned fiber breaks was selected to allow comparison with corresponding Mode I results from LEFM for a crack of length $2c$ in an infinite orthotropic, homogeneous plate in both plane stress and plane strain (see Fig. 1(c)). (In the numerical calculations we will take N to be odd simply for symmetry, though the results will apply for all N.) The BIS analysis still preserves all of the linearly elastic, shear-lag assumptions. In this study, we wish only to calculate the stress concentrations in the local fibers and matrix regions, or we assume that the matrix and fiber strengths are sufficiently high, such that no consequential damage occurs.

To determine fiber and matrix loads and displacements near arbitrarily located fiber breaks in a large unidirectional composite, it is convenient to discretize the composite in the vicinity of these breaks. Unlike say a finite difference scheme, this elastic analysis is exact, and discretization is used merely to establish spatial fiber and matrix points at which to calculate stresses for plotting purposes. Figure 2 shows the two-dimensional lamina of evenly spaced fiber and matrix elements arranged in a brick-like fashion. Each fiber and matrix element is of equal length 2δ, where δ is much less than the characteristic load transfer length, precisely defined later as a certain length required for a broken fiber to recover its applied load. As shown in Fig. 2, the center fiber is numbered $n = 0$, the fibers to the right are numbered $n = 1, 2, \ldots \infty$, and those to the left, $n = -1, -2, \ldots -\infty$. The matrix bay to the right of fiber n is matrix bay n. Likewise, along the loading axis, the respective fiber and matrix elements are numbered in the $+x$ direction from $(n, 0)$ to (n, ∞) and in the $-x$ direction, from $(n, -1)$ to $(n, -\infty)$. Thus (n, m) refers to a specific fiber element or matrix element. We let E be the Young's modulus of the fibers, and G be the effective shear modulus of the matrix. Also w is the effective fiber spacing, h is the fiber width as well as the fiber and lamina thickness, and A is the cross-sectional area of a fiber. (For the ideal case of fibers of square cross-section, $A = h^2$.)

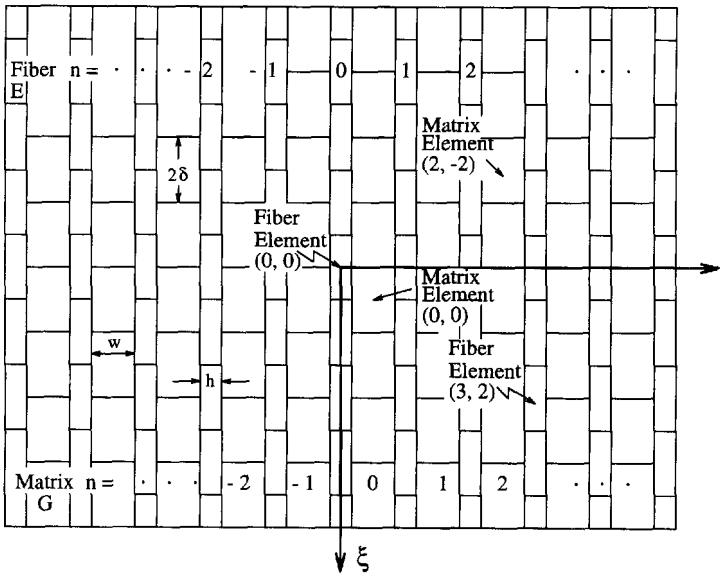

Fig. 2. Two-dimensional discretized composite lamina with equal length and evenly spaced fiber and matrix elements.

The shear-lag assumptions are incorporated when deriving the force equilibrium equations for fiber and matrix elements along the fiber axis, x. Let $p_n(x)$ and $u_n(x)$ be the force and displacement, respectively, in fiber n at location x, and let p^* be the load applied per fiber at $x = \pm\infty$. Since the matrix transmits only shear forces, the shear force per unit fiber length is related to the differential displacements of the two adjacent fibers. The effective shear stress τ_n and the shear strain γ_n in matrix bay n are

$$\tau_n(x) = G[u_{n+1}(x) - u_n(x)]/w \tag{1a}$$

and

$$\gamma_n(x) = [u_{n+1}(x) - u_n(x)]/w, \tag{1b}$$

respectively. Thus, the shear force per unit length applied on the fiber by the matrix is $\tau_n(x)h$. Equilibrium of forces in the x-direction results in the following equilibrium conditions,

$$p_n(x) = EA\frac{\mathrm{d}u_n(x)}{\mathrm{d}x} \tag{1c}$$

and

$$EA\frac{\mathrm{d}^2u_n(x)}{\mathrm{d}x^2} = \frac{-Gh(u_{n+1}(x) - u_n(x)) + Gh(u_n(x) - u_{n-1}(x))}{w}. \tag{1d}$$

For convenience, the above variables are normalized into non-dimensional parameters. The normalized fiber loads P_n, fiber displacements U_n, matrix shear stresses T_n, matrix shear strains Γ_n, and axial coordinate ξ are

$$P_n = p_n/p^*, \tag{2a}$$

$$U_n = \frac{u_n}{p^*\sqrt{\dfrac{w}{EAGh}}}, \tag{2b}$$

$$T_n = \frac{\tau_n}{p^*}\sqrt{\frac{wEAh}{G}}, \tag{2c}$$

$$\Gamma_n = U_{n+1} - U_n = \frac{\gamma_n}{p^*}\sqrt{wEAGh}, \tag{2d}$$

and

$$\xi = \frac{x}{\sqrt{\frac{EAw}{Gh}}}. \tag{2e}$$

Note that since the matrix is deforming elastically, $\tau_n = G\gamma_n$, and thus T_n and Γ_n are equivalent. Also the denominator of (2e) is the characteristic load transfer length referred to earlier.

By introducing these non-dimensional parameters, the equilibrium eqns (1c) and (1d) simplify to,

$$\frac{d^2U_n(\xi)}{d\xi^2} + U_{n+1}(\xi) - 2U_n(\xi) + U_{n-1}(\xi) = 0 \tag{3a}$$

$$P_n(\xi) = \frac{dU_n(\xi)}{d\xi} \tag{3b}$$

and

$$P_n(\pm\infty) = 1, \tag{3c}$$

and on the broken fiber ends the loads are zero, i.e.

$$P_n(0) = 0 \quad \text{for } -(N-1)/2 \leqslant n \leqslant (N-1)/2. \tag{3d}$$

Consequently the form of the solution is independent of the elastic constants and fiber volume fraction, which is $V_f = h/(h+w)$.

Analysis for break influence superposition

The BIS analysis in the shear-lag model allows one to solve for the fiber and matrix stress profiles due to an arbitrary arrangement of fiber breaks in the lamina. In the present work, the locations of the N initial fiber breaks are positioned at the centers of the N fiber elements along the central transverse plane. Determination of the fiber and matrix stresses and displacements everywhere in the lamina builds on a certain solution for a single, isolated fiber break in the elastic lamina at the center of fiber element (0, 0) (see Fig. 3). The solution for the N breaks involves the weighted superposition of N shifted, single break solutions, resulting in a system of N scalar equations to solve for the corresponding weighting factors $K_{b,1}$ to $K_{b,N}$ (Sastry and Phoenix, 1993).

For the problem of a single isolated break, a unit compressive force of magnitude -1 is applied to each end of the break but zero tensile force is applied at $\xi = \pm\infty$ (see Fig. 3). The problem is normalized as described by (2), and we apply the subscript b to distinguish the single break problem from the general problem. Thus the equations to be solved are (3a) and (3b) under the mixed boundary conditions,

$$L_{b,0}(0^+) = -1, \quad L_{b,0}(0^-) = -1 \tag{4a}$$

$$V_{b,n}(0) = 0, \quad \text{for } n \geqslant 1 \quad \text{and } n \leqslant -1, \tag{4b}$$

and

$$\frac{dV_{b,n}(\pm\infty)}{d\xi} = 0, \quad \text{for } -\infty < n < \infty. \tag{4c}$$

Using discrete Fourier transforms, the above equations yield

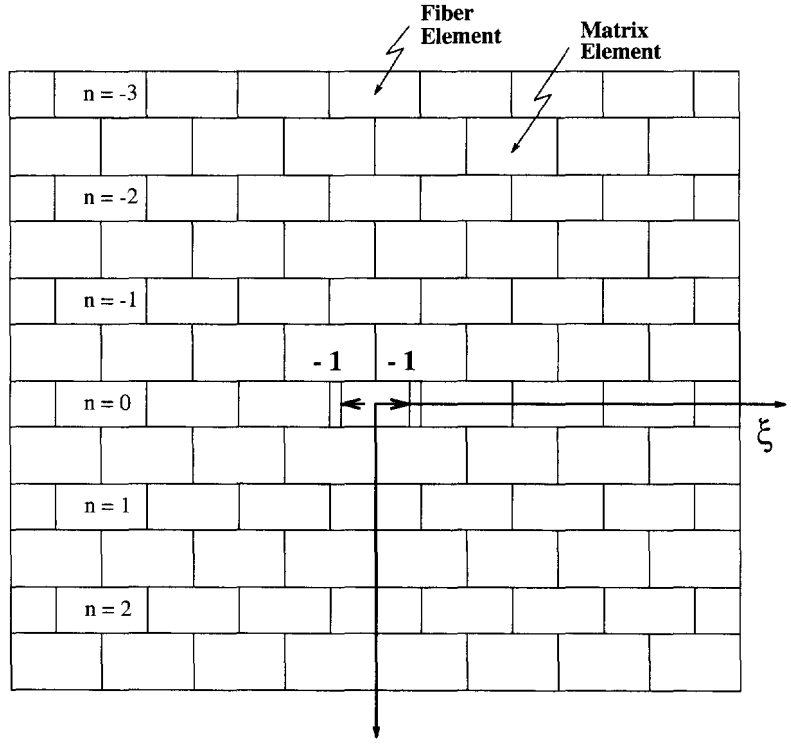

Fig. 3. Single, isolated fiber break at the center of fiber element (0, 0) in the discretized, elastic lamina.

$$V_{b,n}(\xi) = \operatorname{sgn}(\xi)\frac{1}{4}\int_0^{\pi} \cos(n\theta)\, e^{-2|\xi|\sin(\theta/2)}\, d\theta \tag{5a}$$

$$L_{b,n}(\xi) = -\frac{1}{2}\int_0^{\pi} \cos(n\theta)\sin(\theta/2)\, e^{-2|\xi|\sin(\theta/2)}\, d\theta \tag{5b}$$

and

$$\Gamma_{b,n}(\xi) = \operatorname{sgn}(\xi)\frac{1}{4}\int_0^{\pi} \{\cos[(n+1)\theta] - \cos(n\theta)\}\, e^{-2|\xi|\sin(\theta/2)}\, d\theta \tag{5c}$$

where sgn (ξ) is $+1$ if $\xi \geqslant 0$ and -1 if $\xi < 0$. Since these solutions are translation invariant, the solution for an arbitrarily located break at (n_i, ξ_i) is obtained simply by shifting n and ξ in (5) by $-n_i$ and $-\xi_i$ respectively. (Here we have rescaled the longitudinal dimension from m to ξ.) In this way, these shifted solutions are used to determine load transmission factors which in turn can be used to calculate the effects of fiber breaks on the displacements and loads of all the other fibers in the lamina whether broken or not.

The next step is to consider an N-break, auxiliary problem consisting of an infinite lamina containing our N aligned breaks but where each break is loaded on its ends by a compressive force of magnitude -1, and no load is applied at $\xi = \pm\infty$. For this we need load transmission factors from one break to another in the lamina. From the solution to the single break problem, the transmission factor Λ_{ji} is defined as the proportion of load transmitted to the position of fiber break j due to a unit load at fiber break i. Specifically, using (5b) we define

$$\begin{aligned}\Lambda_{ji} &= -L_{b,n_j-n_i}(\xi_j - \xi_i) \\ &= \frac{1}{2}\int_0^{\pi} \cos[(n_j - n_i)\theta]\sin(\theta/2)\, e^{-2|\xi_j-\xi_i|\sin(\theta/2)}\, d\theta.\end{aligned} \tag{6}$$

Thus Λ_{ji} can also be viewed as a proportionality factor, since the proportion of the load on fiber break j transmitted from load $-P_i$ at fiber break i is $-\Lambda_{ji}P_i$. The load transmission factors, Λ_{ji}'s, depend only on the relative distance between respective breaks. Thus, for the N-break problem, the proper weights for each break are determined such that an overall compressive load -1 exists on each fiber break. This requires solution of a system of N equations for the weighting factors $K_{b,1}, \ldots, K_{b,N}$ given in matrix form as

$$\begin{Bmatrix} -P_1 \\ \vdots \\ -P_N \end{Bmatrix} = \begin{bmatrix} \Lambda_{11} & \cdots & \Lambda_{1N} \\ \vdots & & \vdots \\ \Lambda_{N1} & \cdots & \Lambda_{NN} \end{bmatrix} \begin{Bmatrix} K_{b,1} \\ \vdots \\ K_{b,N} \end{Bmatrix}. \tag{7}$$

Thus for the N-break, auxiliary problem, the fiber and matrix loads and displacements at arbitrary position (n, ξ) are the weighted sums of the influences of the N breaks in the laminate. These quantities are given respectively as

$$L_n^*(\xi) = K_{b,1} L_{b,n-n_1}(\xi-\xi_1) + \cdots + K_{b,N} L_{b,n-n_N}(\xi-\xi_N), \tag{8a}$$

$$V_n^*(\xi) = K_{b,1} V_{b,n-n_1}(\xi-\xi_1) + \cdots + K_{b,N} V_{b,n-n_N}(\xi-\xi_N), \tag{8b}$$

$$\Gamma_n(\xi) = K_{b,1} \Gamma_{b,n-n_1}(\xi-\xi_1) + \cdots + K_{b,N} \Gamma_{b,n-n_N}(\xi-\xi_N), \tag{8c}$$

and

$$T_n(\xi) = \Gamma_n(\xi). \tag{8d}$$

Finally, to calculate the desired exact solution for the lamina loaded at $\xi = \pm\infty$ by a tensile force per fiber of unity, a tensile load of unity is superimposed onto the solutions. Thus the dimensionless matrix shear strain Γ_n and stress T_n remain the same, but the fiber loads P_n and displacements U_n become

$$P_n(\xi) = L_n^*(\xi) + 1 \tag{9a}$$

and

$$U_n(\xi) = V_n^*(\xi) + \xi. \tag{9b}$$

To implement the above solution, it is necessary to calculate the integrals in (5a)–(5c) and (6). This was done numerically using a fourth-order Runge-Kutta routine for all points (n, ξ) of interest on the discrete grid in the vicinity of the crack.

For the problem of a single break at (0, 0) under unit compressive load on its ends and no load at infinity, a closed form solution was obtained by Hedgepeth (1961) for the fiber loads along the plane perpendicular to the fibers. He obtained

$$L_{b,n}(0) = \frac{1}{(4n^2-1)}. \tag{10}$$

To check the accuracy of our numerical routine, the percentage differences between $L_{b,n}(0)$ predicted by (10) and by numerical integration in (5b) were calculated for $n \leqslant 600$. The relative errors were rather low. For $n = 100$, 300 and 600, the percentage errors were $5.17 \times 10^{-2}\%$, 0.7453% and 3.6259% respectively. (Note that by $n = 600$, $L_{b,n}(0)$ is only 6.94×10^{-7}.)

Analytically determined stress concentrations

Later, we compare results from the BIS analysis with some analytical results from the shear-lag model. Hedgepeth (1961) calculated the stress concentration factor K_N for the fiber directly adjacent to a row of N breaks. His widely quoted result is

$$K_N = \prod_{j=1}^{N} \frac{2j+2}{2j+1}$$

$$= \frac{2^{2N+1}[(N+1)!]^2}{(2N+2)!}. \tag{11}$$

Hikami and Chou (1990) extended this result by considering the stress concentration on the fibers ahead of the last broken fiber along the crack plane. They obtained stress concentration factor

$$K_{N,s} = (N+2s-1)\frac{(2s)(2s+2)(2s+4)\ldots(2s+2N-2)}{(2s-1)(2s+1)(2s+3)\ldots(2s+2N-1)},$$

$$= \frac{(N+2s-1)2^{2N+1}[(s+N)!]^2(2s-2)!}{(N+s)[(s-1)!]^2(2s+2N)!} \tag{12}$$

which is consistent with Hedgepeth's result since $K_{N,1} = K_N$. On the other hand, Fichter (1969) considered the normalized shear stress concentration S_N in the matrix bay between the last broken fiber and the first intact fiber along the crack plane. That is, he considered $|T_i(0)|$ for $i = (N-1)/2$. He obtained

$$S_N = (\pi/8)\frac{N[(2N)!]}{2^{2N-2}(N!)^2}. \tag{13}$$

Using Stirling's approximation (Ross, 1993)

$$N! \approx \sqrt{2N\pi}N^N e^{-N} \tag{14}$$

for large N, it is a straightforward task to determine asymptotic expressions for these stress concentrations for larger N. We get

$$K_N \approx (\sqrt{\pi}/2)\sqrt{N+1} \tag{15}$$

which proves to be very accurate as the error is about 4% for $N = 2$ and is below 1% by $N \geqslant 10$. Dharani *et al.* (1983) obtained a similar expression, with N in place of $N+1$ in (15). For the shear concentration factor, S_N, we get

$$S_N \approx (\sqrt{\pi}/2)\sqrt{N} \tag{16}$$

which similarly proves to be very accurate. Also using Stirling's approximation (11) for both large N and large s, but $s \ll N$, gives the approximation

$$K_{N,s} \approx \frac{\sqrt{N+1}}{2\sqrt{s-1}}$$

$$\approx \frac{K_N}{\sqrt{\pi(s-1)}}. \tag{17}$$

Equation (17) corresponds to the LEFM solution for a center crack of length $2c$ in an infinite plate. If we take $N+1 = 2c$ and $s-1 = r$, the radial distance from the crack tip, then $K_{N,s} = \sqrt{c/2r}$. We later compare these formulae (11), (13), and (12) with their corresponding approximations (15), (16), and (17). In addition, (12) and (17) are compared to predictions from the exact solution for the normal stresses along the crack plane (Fig. 1(c)).

3. LEFM ANALYSIS IN MODE I

We consider the Mode I LEFM solution for an infinite, two-dimensional, orthotropic composite containing a crack of length $2c$ that is oriented perpendicular to a plane of elastic symmetry and the loading direction (see Fig. 1(c)). In Cartesian coordinates the crack extends through the medium in the z direction and from $-c$ to $+c$ in the y direction, and thus is perpendicular to the x direction, the direction of loading. A remote stress σ^* is applied at $x = \pm\infty$, and the stress results will apply for both plane stress and plane strain (though the displacements for the two cases would differ). In the case of Mode I cracks, the LEFM solution for an orthotropic material uses four elastic material constants, G_{xy}, ν_{yx}, E_{yy}, and E_{xx} (where x corresponds to the fiber direction in later comparisons). Its development involves using the Westergaard approach (Sih, 1981), which consists of a single stress function U, satisfying the fourth-order homogeneous partial differential equation,

$$b_{11}\frac{\partial^4 U}{\partial x^4} + (2b_{21} + b_{66})\frac{\partial^4 U}{\partial x^2\,\partial y^2} + b_{22}\frac{\partial^4 U}{\partial y^4} = 0 \tag{18}$$

where

$$b_{11} = 1/E_{11} = 1/E_{xx} \tag{19a}$$

$$b_{22} = 1/E_{22} = 1/E_{yy} \tag{19b}$$

$$b_{66} = 1/G_{12} = 1/G_{xy} \tag{19c}$$

and

$$b_{21} = -\nu_{21}/E_{22} = -\nu_{yx}/E_{yy}. \tag{19d}$$

The characteristic equation of interest can be written as

$$b_{22}S^4 + (2b_{21} + b_{66})S^2 + b_{11} = 0 \tag{20}$$

where

$$\varepsilon = \frac{b_{22}}{b_{11}} = \frac{E_{11}}{E_{22}} \tag{21a}$$

and

$$\phi^2 = \frac{(2b_{21} + b_{66})}{b_{11}} \tag{21b}$$

so that

$$\varepsilon S^4 + \phi^2 S^2 + 1 = 0. \tag{22}$$

Typically we have $2b_{21} \ll b_{66}$ especially for polymer matrix composites so

$$\phi \approx \sqrt{E_{xx}/G_{xy}}. \tag{23}$$

Normally ε will be considerably greater than unity but for mathematical reasons we will also be interested in the special case where ε is small or when the composite transverse stiffness is very large.

The characteristic eqns (20) or (22) have two usually complex roots S_1 and S_2 of interest (as well as their complex conjugates). For the commonly discussed inner crack tip

stress fields or the K-field with the $1/\sqrt{r}$ singularity, the resulting crack tip stress field equations in terms of polar coordinates, r, the radial distance for the crack tip, and θ, the angle from the crack plane to the point of interest in the x-y plane, are (Sih, 1981)

$$\sigma_x = \frac{K_I}{\sqrt{2\pi r}} \operatorname{Re}\left\{\left(\frac{1}{S_1 - S_2}\right)\left[\frac{S_1}{\sqrt{\cos\theta + S_2 \sin\theta}} - \frac{S_2}{\sqrt{\cos\theta + S_1 \sin\theta}}\right]\right\} \tag{24a}$$

$$\sigma_y = \frac{K_I}{\sqrt{2\pi r}} \operatorname{Re}\left\{\left(\frac{S_1 S_2}{S_1 - S_2}\right)\left[\frac{S_2}{\sqrt{\cos\theta + S_2 \sin\theta}} - \frac{S_1}{\sqrt{\cos\theta + S_1 \sin\theta}}\right]\right\} \tag{24b}$$

and

$$\tau_{xy} = \frac{K_I}{\sqrt{2\pi r}} \operatorname{Re}\left\{\left(\frac{S_1 S_2}{S_1 - S_2}\right)\left[\frac{1}{\sqrt{\cos\theta + S_1 \sin\theta}} - \frac{1}{\sqrt{\cos\theta + S_2 \sin\theta}}\right]\right\}. \tag{24c}$$

In these equations, K_I is the Mode I stress intensity factor and is identical to that for the isotropic case, and thus, is

$$K_I = \sigma^* \sqrt{\pi c}. \tag{25}$$

Note that the tensile stress σ_x ahead of the crack tip along the y-axis ($\theta = 0$) also is identical to those from the isotropic solution (27). Also, the crack tip stress field equations for an orthotropic material typically have the same $1/\sqrt{r}$ singularity as those for an isotropic material. However, the distribution for stresses in the vicinity of the crack tip is more complex and depends on the material's elastic constants.

We also have interest in the complete stress field solution which contains information about both the near crack tip and far field stresses. Later, we compare results from the complete elasticity solution given by Selvarathinam (1995), which was derived from the complex variable approach outlined in Lekhnitskii (1963), to those from the shear lag analysis and the LEFM stress field eqns (24). The purpose is to assess in further detail the true character of any disagreement between the shear lag results and the LEFM results. We note one simple result, which is that the exact solution for the tensile stress, σ_x, along the crack plane (y-axis) for a central crack of length $2c$ in Mode I is

$$\begin{aligned} \sigma_x &= \sigma^* \frac{y}{\sqrt{y^2 - c^2}}, \quad y \geqslant c \\ &= \sigma^* \frac{r + c}{\sqrt{(r + c)^2 - c^2}}, \quad r \geqslant 0. \end{aligned} \tag{26}$$

where $r = y - c$. This stress is also independent of the elastic constants and is the same for both the isotropic problem and orthotropic problem as described. For $r/c \ll 1$ we note the usual $1/\sqrt{r}$ approximation to this result, which is

$$\begin{aligned} \sigma_x &= \sigma^* \frac{\sqrt{c}}{\sqrt{2(y - c)}}, \quad y \geqslant c \\ &= \frac{K_I}{\sqrt{2\pi r}}, \quad r \geqslant 0 \end{aligned} \tag{27}$$

where K_I, given by (25), is the usual stress intensity factor.

Finally we mention some results for the limiting case where $\varepsilon \to 0$, that is when the transverse stiffness E_{22} (along the crack plane) becomes large relative to the longitudinal stiffness E_{11}. In this case one might expect the lateral displacements to reduce to zero and

the solution to have much in common with the shear-lag solution. Asymptotic analysis of the roots S_1 and S_2 of (22) shows they are imaginary and that

$$S_1 \approx \mathrm{i}\frac{1}{\phi}\left\{1-\frac{\varepsilon}{2\phi^4}\right\} \tag{28a}$$

and

$$S_2 \approx \mathrm{i}\frac{\phi}{\sqrt{\varepsilon}}\left\{1-\frac{\varepsilon}{2\phi^4}\right\}. \tag{28b}$$

Note that as $\varepsilon \to 0$, S_1 approaches the constant $\mathrm{i}/\phi = \mathrm{i}/\sqrt{E_{xx}/G_{xy}}$ where the denominator is a key scaling parameter for the shear-lag case, but S_2 approaches $\infty\mathrm{i}$. Through straightforward asymptotic analysis one can show that for the K_I field

$$\sigma_x = \frac{K_I}{\sqrt{2\pi r}}\left(\frac{\cos(\gamma/2)}{(\cos^2\theta+\phi^{-2}\sin^2\theta)^{1/4}}\right)\{1+\sqrt{\varepsilon}/\phi^2+o(\sqrt{\varepsilon})\} \tag{29a}$$

and

$$\tau_{xy} = -\frac{K_I}{\sqrt{2\pi r}}\frac{1}{\phi}\left(\frac{\sin(\gamma/2)}{(\cos^2\theta+\phi^{-2}\sin^2\theta)^{1/4}}+\mathrm{error}(\varepsilon,\phi,\theta)\right) \tag{29b}$$

where

$$\tan\gamma = \phi^{-1}\tan\theta, \tag{29c}$$

and where

$$\mathrm{error}(\varepsilon,\phi,\theta) = O(\varepsilon^{1/4}/\sqrt{\phi}) \quad \text{for } \theta \gg \theta_{\varepsilon,\phi} \approx \sqrt{\varepsilon}/\phi \tag{29d}$$

but

$$\mathrm{error}(\varepsilon,\phi,\theta) = O(1) \tag{29e}$$

for small $\theta_{\varepsilon,\phi} \approx \sqrt{\varepsilon}/\phi$ near the origin, which tends to zero as ε tends to zero. Note that for $\theta = 0$, $\tau_{xy} = 0$, but for $\theta \approx \theta_{\varepsilon,\phi}$, there is a sharp fluctuation in the sign of τ_{xy}. In other words, when $x > 0$, $\tau_{xy} > 0$ and rises and falls over a range of approximately $0 < \theta \leqslant \theta_{\varepsilon,\phi}$, and $\tau_{xy} < 0$ for $\theta_{\varepsilon,\phi} < \theta \leqslant \pi/2$. Therefore as $\sqrt{\varepsilon}/\phi$ tends to zero, the range of θ near the crack plane where τ_{xy} oscillates diminishes, but does not vanish.

On the other hand, it turns out that

$$\sigma_y = \frac{K_I}{\sqrt{2\pi r}}\{1/\sqrt{\varepsilon}+O(1)\} \quad \text{at } \theta = 0 \tag{29f}$$

that is, along the crack plane and

$$\sigma_y = \frac{K_I}{\sqrt{2\pi r}}\{1/(\varepsilon^{1/4}\sqrt{2}\phi^{3/2})+O(1)\} \quad \text{at } \theta = \pi/2 \quad \text{and } r > 0 \tag{29g}$$

and hence σ_y grows unbounded as $\varepsilon \to 0$. Later, we will see that σ_y looks like a spike as $\varepsilon \to 0$, and also we compare (29f) and (29g) with the σ_y stress field equation (24b) to show that these formulas indeed capture the behavior of σ_y as $\varepsilon \to 0$.

Finally we note that some of the above errors are connected to the value of the parameter $\varepsilon = E_{xx}/E_{yy}$, and in (29a) and (29d) the error is proportion to $\sqrt{\varepsilon}/\phi^2$. But from (23)

$$\sqrt{\varepsilon}/\phi^2 \approx G_{xy}/\sqrt{E_{xx}E_{yy}}. \tag{29h}$$

Typically, G_{xy} is much less than E_{xx} for a polymer matrix composite relative to a metal

matrix composite, and therefore, by (30), the error should be less for the polymer matrix composite. For both cases this error dies out as E_{yy} is increased i.e. as $\varepsilon \to 0$.

4. FRAMEWORK OF COMPARISON OF SHEAR-LAG AND LEFM RESULTS

A major objective of this study was to determine the regions and conditions for good agreement between the shear-lag and the LEFM solutions for a center-cracked homogeneous, orthotropic composite. Both approaches are two-dimensional analyses, where the fracture mechanics stress formulation assumes plane stress or plane strain (the stresses are the same for both but the displacements differ), but the shear-lag model specifically assumes neither (though the fiber and matrix moduli can be interpreted and adjusted perhaps to accommodate one or the other). In order to study Mode I crack behavior, an initial crack is modeled in the shear-lag case as a row of N contiguous fiber breaks and in the case of LEFM as a crack of length $2c$. For the LEFM inner crack tip stress solution for a continuum to reasonably match the shear-lag solution for a discrete lamina, one might anticipate that the crack length should be large compared to the crack tip zone being studied, where the latter is at least the scale of one fiber diameter. In the lamina, we considered cases of N ranging from about 20 to 301 contiguous fiber breaks in the transverse central "crack". Although the analysis and numerical routines can handle $N > 300$, the upper limit of $N = 301$ was sufficient for making a comprehensive and valid comparison between the two solutions for a minimal amount of computation time.

In addition to the inner crack tip field, another interest was in how the fiber and matrix stresses actually compare farther from the crack tip in both models (where LEFM $1/\sqrt{r}$ behavior alone would be inaccurate). For the shear-lag analysis, this may apply to examining the stresses outside of a potential plastically yielded or debonded region, but in the LEFM analysis, the $1/\sqrt{r}$ approximation ceases to be valid at large distances from the crack. Therefore, we also consider numerical results for the full elastic field in the homogeneous problem.

Comparing these two different modeling approaches, LEFM and shear-lag, requires defining an equivalent crack length and relating the elastic constants between a composite lamina with discrete fibers of diameter h and matrix regions of width w and those of an orthotropic, homogeneous continuum. Figure 1 exhibits three ways to view the material system: (a) a lamina containing equally spaced fibers and matrix regions, (b) a material with tension lines and shear stress regions of width w^*, and (c) an orthotropic continuum. The shear-lag model assumes all the unbroken fibers remain laterally rigid and straight, but in reality, the fibers ahead of the crack tip bend and rotate somewhat due to varying local transverse normal stresses. In the present work, results from the shear-lag stress analysis are examined with respect to Fig. 1(b). In Fig. 1(b), a fiber (and any axial tension carrying ability of the matrix) has been mathematically collapsed to a tension line with an effective stiffness EA, and the matrix has been widened (though given a higher stiffness $G(h+w)/w$ to compensate) with spacing $(w+h)$ in place of w. The mathematical analysis using Fig. 1(b) is identical to that using Fig. 1(a).

In comparing the two solutions we study the behavior of the three main crack tip stresses: (1) the normal stress, σ_x, decaying along the crack plane (y-axis) ahead of the crack tip, (2) the shear stress, τ_{xy}, in the matrix bays vs the fiber axial distance x, and (3) the fiber stress, σ_x, vs fiber axial distance, x. We also calculate the transverse stress σ_y in order to see its magnitude near the crack tip and to determine the extent to which these stresses can actually be supported in an actual composite without local debonding.

Crack length

For the discrete lamina, the crack length is modeled as an effective width of broken fiber and matrix bays. Specifically, for a given number of N fiber breaks, the equivalent crack length $2c$ consists of $(N-1)$ effective spacings of width $(h+w)$, plus two end portions, each the fraction $1-\Phi$ of $(h+w)$, which extend into the matrix bays between the last broken fiber and first intact fiber on both sides of the crack, as shown in Fig. 1(b). That is, writing c_N in place of c,

$$2c_N = [(N-1)+2(1-\Phi)](h+w). \tag{30}$$

Thus Φ is a small adjustment, being the fraction of the width $(h+w)$ between the centerline of the first surviving fiber back to the crack tip. Φ will be determined empirically by matching the decay of σ_x along the crack plane ahead of the crack for the LEFM and shear-lag BIS solutions.

Elastic material constants

As discussed earlier, the LEFM solutions for the crack-tip stress fields depend on the orthotropic material's elastic constants G_{xy}, v_{yx}, E_{yy}, and E_{xx}. On the other hand, in the shear-lag analysis, solutions are in terms of non-dimensional quantities: the normalized loads P_n, the shear stresses T_n, and the fiber axial distance ξ. Calculating the physical quantities p/p^*, τ, and x from P_n, T_n, and ξ, requires values for the fiber and matrix parameters, E, G, A, w, and h in (2). To make contact with the LEFM solution, we must determine "effective" values for the elastic constants, namely $G^*_{xy}, v^*_{yx}, E^*_{yy}$, and E^*_{xx}. For this purpose we assume isotropic fibers and matrix with respective elastic constants E_f, $G_f = E_f/[2(1+v_f)]$ and v_f, and E_m, $G_m = E_m/[2(1+v_m)]$ and v_m, and use the simple rule-of-mixtures formulas in terms of fiber volume fraction V_f. These are

$$E^*_{xx} = E_f V_f + E_m(1-V_f) \tag{31a}$$

$$1/G^*_{xy} = V_f/G_f + (1-V_f)/G_m \tag{31b}$$

$$1/E^*_{yy} = V_f/E_f + (1-V_f)/E_m \tag{31c}$$

and

$$v^*_{yx} = (E^*_{yy}/E^*_{xx})(v_f V_f + v_m(1-V_f)). \tag{31d}$$

Actually, we can extend the shear-lag model to write the governing equations in terms of the above constants. In this extension we are assuming that any tensile load carried in the matrix is lumped in with the fiber and any shear deformation in the fiber is lumped in with the matrix (see Fig. 1(b)). Then we have $V_f = h/(h+w)$, and the effective shear modulus G^*_{xy}, Young's modulus, E^*_{xx}, cross-sectional area $A^* = h(h+w)$, and effective matrix spacing, $w^* = h+w$ replace G, E, A, and w, respectively, in (1) and (2). Also note that σ and σ^* correspond to p/A^* and p^*/A^*, respectively. These replacements effectively "smear" (or homogenize) the geometric and elastic material properties of the matrix and fibers, but also lump them into appropriate slots in the shear-lag model.

One might anticipate that when E^*_{yy} is very large, the agreement between the LEFM model and the shear-lag model will improve. In the orthotropic continuum of the LEFM model, we note that transverse deformation is affected by E^*_{yy}. Intuitively, an infinitely stiff transverse stiffness restricts both the unbroken and broken fibers to displace only in the fiber direction as assumed in the shear-lag analysis. Mathematically, when E^*_{yy} is large or ε is small, the fourth order equilibrium equation (18) collapses to a second order equation dependent only on E^*_{xx} and G^*_{xy}, and therefore, the solution has a similar form to that of the shear-lag analysis (3). In this respect the rule of mixtures can considerably underestimate E^*_{yy} when there are actually local constraints, such as other lamina layers, preventing local matrix contraction in the z direction.

In examining the extent to which agreement in the fiber tensile stresses and matrix shear stresses depends on the material system, two types of unidirectional composites were considered: a graphite or carbon fiber/polymer-matrix composite and a ceramic fiber/metal-matrix composite. Consistent with the shear-lag model assumptions, the fiber stiffness is significantly higher than the matrix stiffness in both types of composites, namely 100 : 1 for the polymer-matrix composite and 3 : 1 for the metal-matrix composite. The resulting effective elastic constants calculated from (31) and geometric properties used for these two

Table 1. Stiffness constants for the two composites considered in example calculations

	Metal matrix	Polymer matrix
E^*_{xx}	266.7 GPa	50 GPa
G^*_{xy}	76.93 GPa	2 GPa
E^*_{yy}	200 GPa	4 GPa
ν_{yx}	0.225	0.024
V_f	0.50	0.50

types of unidirectional composites are listed in Table 1. (In later discussion all elastic constants will be in units of GPa.)

Next we draw a connection between the results for stress concentration factors in the shear-lag model and LEFM. To develop a correspondence we recall that in the case of the LEFM model, we plot results in terms of y/c and σ/σ^*. In the shear-lag model, the y direction is again normalized to y/c_N where

$$c_N = [(N-1)+2(1-\Phi)]w^*/2 \cong Nw^*/2 \tag{32}$$

according to (30), and thus $2c \approx Nw^*$. Next we define

$$r_s = [\Phi+(s-1)]w^*. \tag{33}$$

Then the earlier result (27) from LEFM with r_s in place of r can be written

$$(K_{N,s})_{cont.} = \frac{\sigma}{\sigma^*} = \sqrt{\frac{c}{2r}} \approx \frac{\sqrt{N+1}}{2\sqrt{s-1}} \tag{34}$$

which agrees with the result (17) from shear-lag theory.

Finally we determine a scaling to compare the shear-lag and LEFM solutions along the fiber direction (x-axis). For the shear-lag model, in the longitudinal direction we must convert from ξ to x. Using (2e) and the above relations we find

$$x = \xi w^* \sqrt{\frac{E^*_{xx}}{G^*_{xy}}}. \tag{35}$$

Thus both the shear-lag model and the LEFM model point to the importance of a parameter

$$\phi' = \sqrt{E^*_{xx}/G^*_{xy}}. \tag{36}$$

In the shear-lag model this is clear from (35) so that

$$x = \xi w^* \phi', \tag{37}$$

whereas in the LEFM model the parameter ϕ' was actually ϕ given by (21b). For many fiber reinforced composites and especially the two types considered in the present work, the approximation (23), $\phi \approx \sqrt{E^*_{xx}/G^*_{xy}}$, is typically extremely close to the true ϕ. Thus we propose the use of the coordinate

$$\begin{aligned} \xi_{c_N} &= x/(c_N\phi') \\ &\approx 2\xi/N \end{aligned} \tag{38}$$

for the shear-lag case and $\xi_c = x/(c\phi')$ for the LEFM case when plotting the results in the axial x direction. Thus we have determined scales to plot the results p_n/p^* and τ_n/p^*, which correspond to σ_x/σ^* and τ_{xy}/σ^*, respectively, using the Cartesian coordinates y/c_N and x/c_N. For the two types of composites in Table 1, $\phi_{polymer} = 5 \geqslant \phi_{metal} = 1.86$. As a last point, σ_x

and τ_{xy} in the LEFM model correspond to $p_n/(w^*h) = p_n/A^*$ and τ_n respectively, in the shear-lag model. Now we will consider the extent to which the normalized shear-lag stress profiles match the LEFM profiles.

5. RESULTS AND DISCUSSION

This section presents typical results for the crack plane tensile stresses and the crack-tip stresses along the fiber direction ξ_c for a lamina containing a central crack of various lengths as predicted by the shear-lag, LEFM, and complete elasticity solutions.

Tensile stresses along the crack plane

As mentioned, comparing the LEFM with the shear-lag stress distributions requires defining an equivalent crack length (30) given the number of fiber breaks N and an unknown parameter Φ. An appropriate value for Φ, the portion of the intact matrix bay on either end of the crack, is determined based on the crack plane tensile stresses, σ_x for $\theta = 0$ and varying r. We selected Φ such that in the vicinity of the crack tip, the two solutions agreed down to the scale of about one fiber spacing w^* for longer crack lengths. In this case, the tensile stresses along the crack plane calculated from the orthotropic LEFM solution are independent of the material's elastic properties and therefore, are the same as those calculated in the isotropic case. As a result, the best fit Φ value is completely independent of the material's elastic properties and N, when N is large (i.e. $N \geqslant 100$). Using log-log coordinates, Fig. 4 compares the crack tip tensile stress concentrations σ/σ^* and p/p^* calculated from the exact solution (26), LEFM $1/\sqrt{r}$ solution (27), and the shear-lag approach, respectively, for $N = 301$ and different values of Φ. The horizontal coordinate is r_s for the shear-lag solution and $r = y - c$ for both the exact and the LEFM $1/\sqrt{r}$ solutions, and the vertical coordinate is the corresponding stress concentrations divided by $\sqrt{c}$. Note that for the shear-lag model, the plot begins at $r_1 = \Phi w^*$, the location of the center of the first surviving fiber ahead of the crack. Since this radial distance is less than one fiber diameter, smaller values of r have no real meaning in either model. In the shear-lag model, the matrix material does not sustain a tensile load, and in the LEFM model, these stresses are high due to the $1/\sqrt{r}$ singularity. Furthermore, at such a length scale of less than a fiber diameter, the unidirectional composite cannot be modeled as an orthotropic continuum. Clearly, from Fig. 4, $\Phi = 1/3$ yields good agreement for crack lengths $c = c_N$ down to about

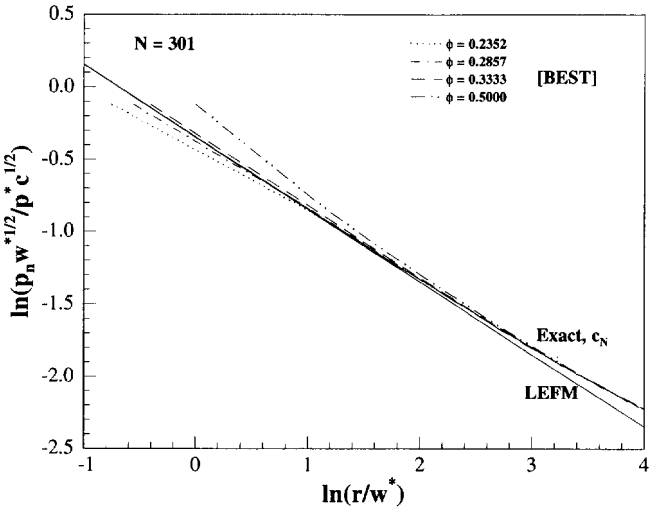

Fig. 4. Normal tensile stresses along the crack plane predicted from (26), (27), and the shear-lag analysis for $N = 301$ and different Φ in (30).

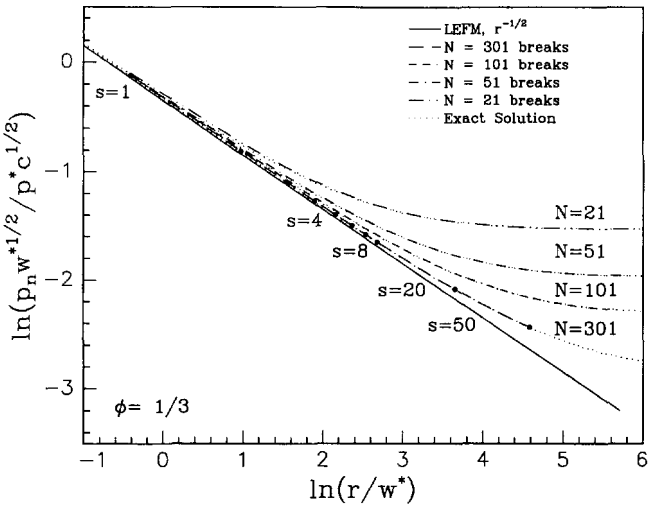

Fig. 5. Normal tensile stresses along the crack plane predicted from (26), (27), and the shear-lag analysis for $\Phi = 1/3$ and different N, number of fiber breaks.

$N = 21$ where adjustments become necessary. Figure 5 shows similar plots of the same fiber σ/σ^* and p/p^* calculated from the LEFM $1/\sqrt{r}$, exact, and shear-lag solutions vs r and r_s for N ranging from 21 to 301 and for $\Phi = 1/3$. Figure 5 shows the outstanding agreement between the shear-lag solution and the exact solution, even in the far field region ($s \geqslant 20$), where LEFM $1/\sqrt{r}$ is not valid. Near the crack tip, the stress distributions for all three solutions vary as $1/\sqrt{r}$. For instance, for $N = 301$, the two solutions reasonably agree for $s \leqslant 8$, after which the shear-lag curve follows the exact solution over the entire range of r shown. Furthermore, as the number of breaks increases above $N \geqslant 101$, the range of r where there is little or no difference between the results of the three solutions lengthens and becomes less sensitive to the value of Φ. On the other hand, for shorter crack lengths, $N \leqslant 21$, agreement between the predictions from the shear-lag and both the LEFM and exact solutions becomes poorer and the best fit value for Φ starts to depend on N. These results suggest that the LEFM solution really fails to work properly in this domain since the scale of discrete fibers and matrix is too coarse.

In Table 2, we compare the K_N (11) and S_N (13) formulae with their corresponding approximations (15) and (16). The tabulated results show excellent agreement; for K_N, the error is 4% for $N = 2$ and decreases to below 1% for $N > 10$. Similar trends are observed for S_N, but the error is slightly higher than that of K_N (less than 0.1%). Table 3 compares results from the formula (13) for $K_{N,s}$, the stress concentration on the sth intact fiber ahead of N fiber breaks, with the exact solution (26), and the corresponding approximation (17). Overall, the agreement between $K_{N,s}$ and the exact solution is outstanding for $N \geqslant 5$. Also, from Table 3, the approximation to $K_{N,s}$, which assumes N is sufficiently large and $1 \ll s \ll N$, deviates between 1 and 5% from (13) for $s/N \leqslant 0.1$ when $N > 20$ and for $0.05 < s/N < 0.0833$ when $N \geqslant 50$. In fact, the differences between $K_{N,s}$ and its corresponding approximation (17) are similar to those between the exact solution and the LEFM $1/\sqrt{r}$ approximation. The reason is that the primary assumption of $s/N \ll 1$ in (17) is analogous to the $r/c \ll 1$ validity criterion for the LEFM $1/\sqrt{r}$ approximation (27).

Tensile stresses along the fiber direction

Next, we compare the stress fields for a crack of length $2c_N$ with $N = 301$ and for various choices of r_s where $s = 1$, 2, 5, and 20. Results are given for the shear-lag solution, the complete elasticity solution, and the $1/\sqrt{r}$ LEFM solution. Using (38), the x coordinate is normalized to $\xi_{c_N} = x/(c_N\phi') \approx 2\xi/N$ and $\xi_c = x/(c\phi')$. Figures 6 and 7 plot the tensile stress concentrations along the fiber direction for the two composites, the polymer-matrix, fiber composite and the metal-matrix, fiber composite, respectively, with properties listed in Table 1. In the shear-lag model, the stress concentration reaches a peak significantly above unity at $\xi_c = 0$ (i.e. the crack plane) and gradually decays as the fiber recovers its

Table 2. Exact and approximate values for fiber (K_N) and matrix (S_N) load concentrations next to N breaks

N	K_N, eqn (11)	K_N, eqn (15)	% error
1	1.333	1.253	6.00
2	1.600	1.535	4.06
3	1.829	1.773	3.07
4	2.032	1.981	2.46
5	2.217	2.171	2.06
10	2.973	2.939	1.13
30	4.954	4.934	0.40
50	6.344	6.329	0.24
80	7.988	7.976	0.15
N	S_N, eqn (13)	S_N, eqn (16)	% error
1	0.735	0.886	12.84
2	1.178	1.253	6.39
3	1.473	1.535	4.24
4	1.718	1.773	3.17
5	1.933	1.982	2.53
10	2.768	2.803	1.26
30	4.834	4.854	0.42
50	6.251	6.267	0.25
80	7.914	7.927	0.16

Table 3. Exact and approximate values for fiber load concentrations on the sth fiber away from N contiguous breaks

	s	Exact eqn (26)	$K_{N,s}$ eqn (12)	$K_{N,s}$ eqn (17)	% error (12) and (17)
$N = 1$					
	2	1.061	1.066	0.707	33.7
	3	1.026	1.029	0.500	51.4
	4	1.014	1.016	0.408	59.8
	5	1.009	1.010	0.354	0.65
$N = 5$					
	2	1.342	1.364	1.225	10.2
	3	1.182	1.193	0.866	27.4
	4	1.116	1.123	0.707	37.1
	5	1.082	1.086	0.612	43.6
$N = 10$					
	2	1.648	1.680	1.658	1.3
	3	1.380	1.396	1.173	16.0
	4	1.259	1.267	0.957	24.6
	5	1.192	1.199	0.829	30.8
$N = 30$					
	2	2.539	2.595	2.784	7.3
	3	2.004	2.033	1.969	3.2
	4	1.746	1.764	1.607	8.9
	5	1.591	1.603	1.392	13.2
$N = 50$					
	2	3.193	3.265	3.571	9.9
	3	2.481	2.517	2.525	0.3
	4	2.131	2.153	2.062	4.3
	5	1.917	1.932	1.785	7.6
$N = 80$					
	2	3.977	4.068	4.500	10.6
	3	3.061	3.105	3.182	2.5
	4	2.605	2.633	2.598	1.3
	5	2.323	2.343	2.250	4.0

load of p^* at $x = \pm\infty$. On the first intact fiber, $s = 1$, the two solutions achieve excellent agreement for both the polymer and the metal matrix composite. For subsequent fibers, the maximum stress for both the LEFM $1/\sqrt{r}$ approximation and the complete solution does not occur along the crack plane, but at a small distance on both sides of the crack plane. As we point out in the next section which compares shear stress results, a rapid

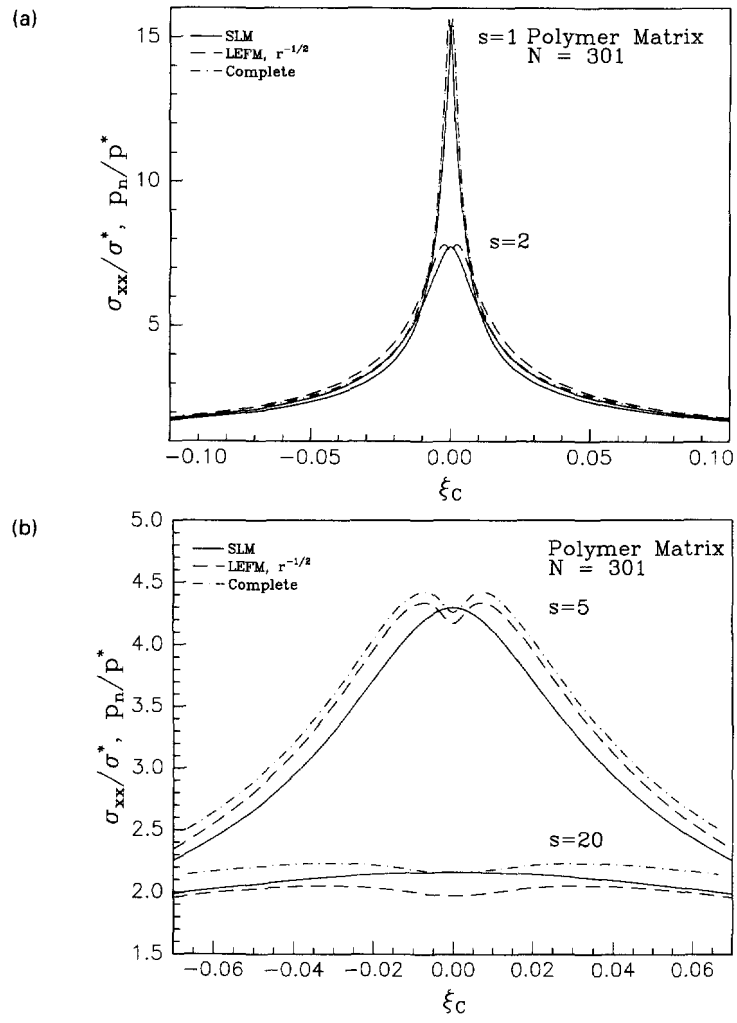

Fig. 6. Fiber tensile stress concentrations along (a) the axis of the 1st and 2nd fibers, and (b) along the axis of the 5th and 20th fibers in a polymer-matrix composite predicted from the shear-lag analysis, LEFM, and the complete solution.

double oscillation in the τ_{xy} profile near the crack plane ($\xi_c = 0$) causes a slight "dip" in the load profile of the adjacent fiber. Since the range of θ over which this "offset maximum" occurs is fixed by material constants, this phenomenon occurs over a more substantial fiber length on fibers further away from the crack tip. This perhaps provides another explanation as to why cracks in anisotropic materials with statistical flaws would tend to grow nonplanar. In the next section, we also show that the τ_{xy} oscillation does not appear in the matrix bay containing the crack tip ($n = 1$), which explains why this "dip" in σ_x does not occur in first surviving fiber (Figs 6(a) and 7(a)).

Figure 8 shows the same results on a log-log scale to better observe the $1/\sqrt{r}$ behavior for a polymer matrix composite. As seen previously, for r_1 the agreement is excellent but the agreement weakens as r_s increases in s, where the stresses in the both the complete and LEFM cases tend to "rise" slightly when traveling away from the crack plane before decaying. Therefore, the decay behavior of the two solutions is similar, but the LEFM is delayed in $|\xi|$ relative to the shear-lag case. Note that for $s = 20$ or $r_s/c_N = 0.128$, the shear-lag results lie between those from the LEFM $1/\sqrt{r}$ and the complete elasticity solutions, and therefore, the discrepancy is no worse than the discrepancy between the complete and LEFM $1/\sqrt{r}$ solutions.

Figure 9 compares the fiber stress concentrations at point r approximately $r/c_N = 0.05$ away from the crack tip for $N = 51$ and $N = 301$. Using a modified Φ for $N = 51$ and $\Phi = 1/3$ for $N = 301$, the two solutions produce nearly the same profiles. Also note that

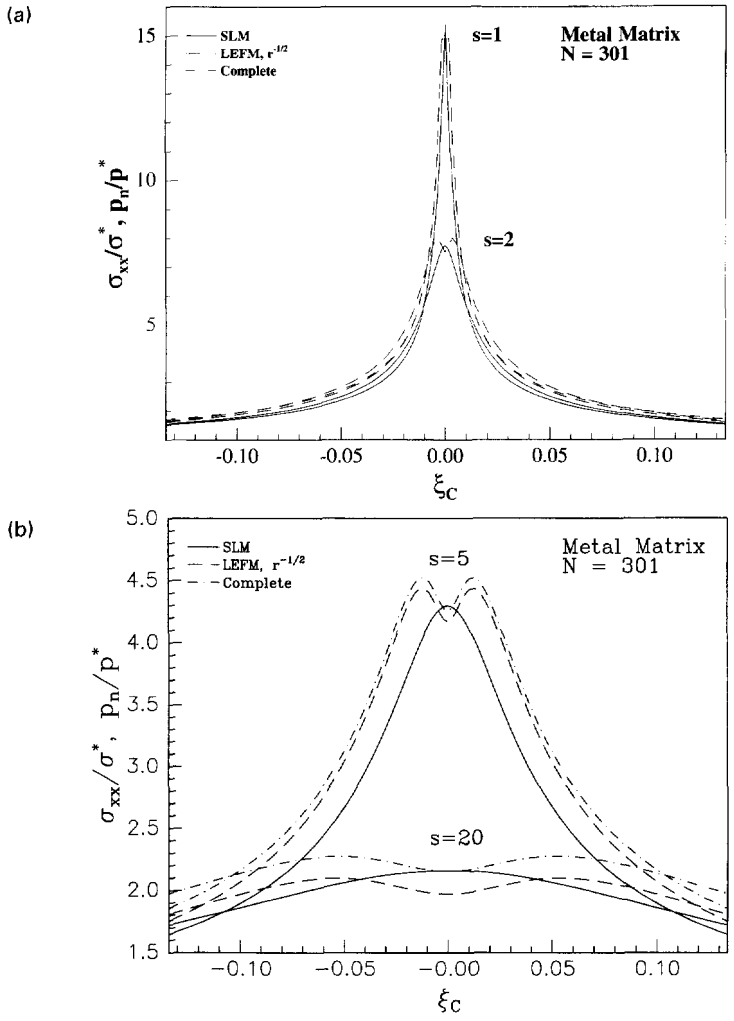

Fig. 7. Fiber tensile stress concentrations along (a) the axis of the 1st and 2nd fibers, and (b) along the axis of the 5th and 20th fibers in a metal-matrix composite predicted from the shear-lag analysis, LEFM, and the complete solution.

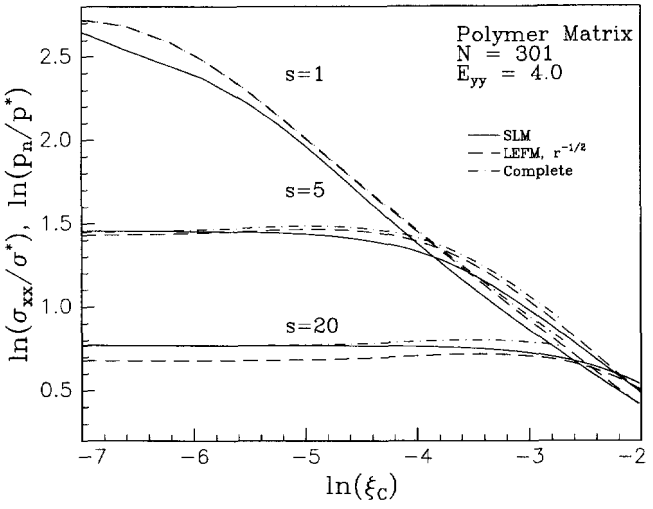

Fig. 8. Log-log plot of fiber tensile stress concentrations along the axis of the 1st, 5th, and 20th fibers in a polymer matrix composite predicted from the shear-lag analysis, LEFM, and the complete solution.

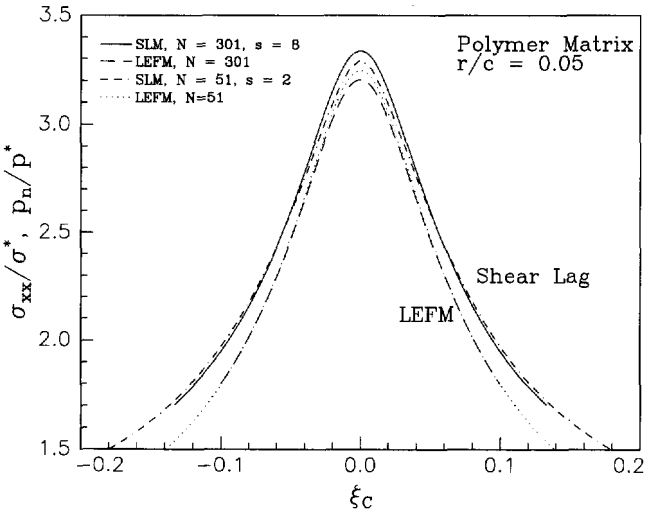

Fig. 9. Fiber tensile stress concentrations at $r/c_N = 0.05$ in a polymer matrix composite for $N = 301$ and $N = 51$ predicted from the shear-lag analysis and LEFM.

the two LEFM curves converge and the two shear-lag curves converge at a slight distance away from the crack tip.

Earlier analysis leading to (29a) indicated that the relative discrepancy in σ_x is given by the value of $\sqrt{\varepsilon}/\phi^2 \approx G_{xy}/\sqrt{E_{xx}E_{yy}}$. Since, typically, $E_{xx} \ll G_{xy}$ in a polymer-matrix composite, the error should be less for the polymer-matrix composite than the metal-matrix composite and should die out in both cases as E_{yy} is increased. Figure 10 shows a normalized plot of the stress concentrations in fiber $s = 5$ ahead of $N = 301$ breaks using various values of E_{yy} (= 4, 100, and 10^8) or $\sqrt{\varepsilon}/\phi^2 \approx G_{xy}/\sqrt{E_{xx}E_{yy}}$ (= 0.1414, 0.028, and 2.8×10^{-5}) for the polymer matrix composite. This point corresponds to $r/c = 0.0288$ ahead of the crack along the crack plane and thus, $r/c > 0.0288$ when traveling along the fiber. In this particular case, we find that reducing the error to a negligible amount requires $\varepsilon = E_{xx}/E_{yy} < 5 \times 10^{-4}$. As E_{yy} is increased, the maximum fiber stress in the LEFM $1/\sqrt{r}$ calculation occurs at the crack plane, but at a slightly lower value than that of the shear-lag model. This difference is explained in Fig. 5, which shows the faster decay rate characteristic of the $1/\sqrt{r}$ approximation. Figure 5 also points to the fact that the maximum fiber stress is extremely close to that predicted from the exact solution (26). Figure 11 shows excellent agreement between the two solutions when $E_{yy} = 10^8$ in the LEFM solution for fiber $s = 1$ up to fiber $s = 10$.

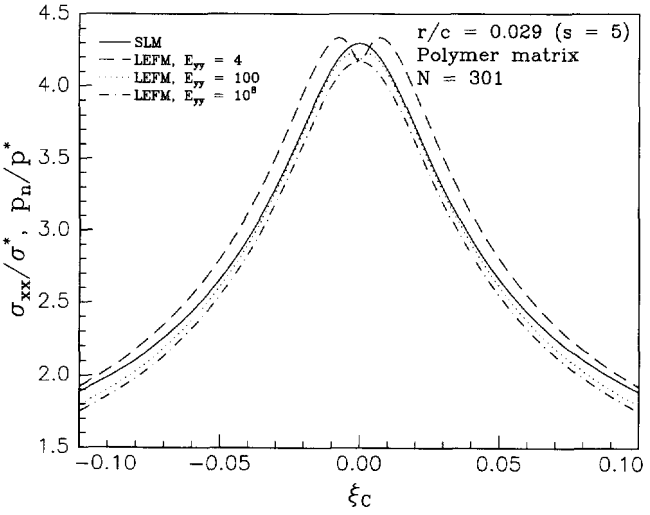

Fig. 10. Fiber tensile stress concentrations along the axis of the 5th fiber ahead of $N = 301$ fiber breaks predicted from LEFM for various values of E_{yy} and the shear-lag analysis.

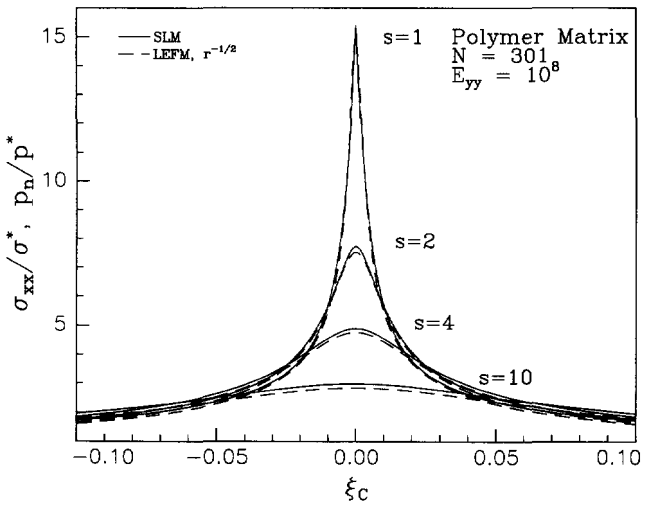

Fig. 11. Fiber tensile stress concentrations along the axis of the 1st, 2nd, 4th, and 10th fibers ahead of $N = 301$ fiber breaks in a polymer-matrix composite predicted from LEFM with $E_{yy} = 10^8$ and the shear-lag analysis.

Similarly, when plotting the results on log-log coordinates (Fig. 12), excellent agreement is observed in the decay behavior of the two solutions.

Equation (30) indicates that the error is much smaller when $E_{xx} \gg G_{xy}$. Therefore, as we expected, similar trends are observed for a metal-matrix composite, but for much smaller values of ε, since $\phi^2 = E_{xx}/G_{xy}$ is typically smaller in a metal-matrix composite. In a metal-matrix composite, typically $E_{yy} \approx (2 \text{ or } 3)G_{xy}$ so $\sqrt{\varepsilon}/\phi^2 \approx \sqrt{G_{xy}/(2E_{xx})} = 1/(\sqrt{2}\phi)$, so the value of $\varepsilon = E_{xx}/E_{yy}$ must be about 2 to 8 times smaller than for the polymer matrix composite. To achieve the same agreement, we find that $\varepsilon = 5 \times 10^{-7}$ for the polymer matrix and $\varepsilon = 2.67 \times 10^{-7}$ for the metal matrix composite.

Shear stresses along the fiber direction

We now compare the matrix stress τ_{xy} predictions from the shear-lag and both the LEFM model and complete elasticity solution for a crack of length $2c_N$ with $N = 301$ and for various choices of r_s where $s = 1$, 2, and 5. Given r_s the τ_{xy} calculation is for the matrix bay $s-1$ which is just to the left of fiber s ahead of the last broken fiber. In the shear-lag analysis, τ_{xy} exists only in the matrix region and within a given matrix bay n, and remains

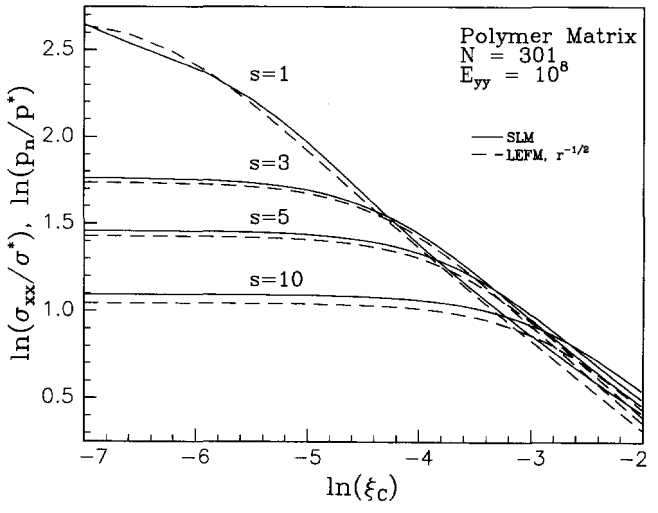

Fig. 12. Log-log plot of the fiber tensile stress concentrations along the axis of the 1st, 3rd, 5th, and 10th fibers ahead of $N = 301$ fiber breaks in a polymer-matrix composite predicted from LEFM with $E_{yy} = 10^8$ and the shear-lag analysis.

constant with respect to y. Therefore, τ_{xy} calculated within matrix bay n only varies with the fiber axial distance, x. Therefore, it is valid to compare the shear-lag shear stress profile, τ_{xy} vs ξ_c, in matrix bay n with that of the LEFM results at all distances r ahead of the crack tip within matrix bay n. Results are given for the shear-lag solution, the complete elasticity solution, and the LEFM $1/\sqrt{r}$ solution, and as in the tensile loads, the x coordinate is normalized to $\xi_{c_N} = x/(c_N\phi') \approx 2\xi/N$ for the shear-lag results and $\xi_c = x/(c\phi')$ for the LEFM $1/\sqrt{r}$ and complete elasticity solution results. Figures 13 and 14 plot the shear stress concentrations (shear stress τ_{xy} divided by far field tensile stress σ^* or $p^*/(w^*h)$) along the fiber direction for the polymer matrix composite and the metal-matrix composite, respectively, with properties as listed in Table 1. In all cases, the matrix bay surrounding the crack tip experiences the highest shear stresses small distances ξ_c away from the crack plane. Within this matrix bay, the agreement between the two solutions is very good when the shear-lag shear stresses are evaluated far from the crack tip. However, the agreement weakens as r_s increases in s. In subsequent matrix bays, the LEFM τ_{xy} undergoes a rapid sign change near the crack plane or tends to oscillate sharply for one cycle when traveling away from the crack plane before decaying. According to (29e), this phenomenon is expected and diminishes (but fails to die out completely) as $\varepsilon \to 0$. In agreement with (24c) and (29e), when traveling away from the crack, the rapid shear reversal decreases in magnitude as $1/\sqrt{r}$ but occurs over a larger fiber length, since the θ range over which the oscillation occurs is fixed by material constants. Therefore, agreement in the shear stresses in the far field region does not improve. Considering that in the far field region, the LEFM $1/\sqrt{r}$ solution ceases to be valid and the shear stresses are insignificant ($\tau_{xy} \leqslant 0.1$) relative to those created in the crack tip region, disagreement is expected. In the two dimensional lamina, this single oscillation, where the peak shear stress rapidly changes from positive to negative, would occur over several fiber diameters. Note, however, that the peak shear stress of the oscillation is much less than the maximum shear stress in the first matrix bay. Figures 13 and 14 also show that the maximum shear stress in the shear-lag τ_{xy} is slightly higher and closer to the crack plane than that for LEFM τ_{xy}. In subsequent bays the decay for LEFM is similar but delayed in $|\xi|$ relative to the shear-lag case. Note that the discrepancy is larger than in the case of σ_x. Aside from the near crack plane oscillation, reasonable agreement between the shear stress profile of the two solutions and for the polymer and metal matrix composites can be achieved within 10 matrix regions or within the crack tip region. In addition, both analyses show the same axisymmetric profile, reduction in the maximum shear stress, and shift away from the crack plane of the location of the maximum shear stress.

Earlier analysis before (29h) suggests that the relative discrepancy in τ_{xy} is generally given by the value of the parameter $\sqrt{\varepsilon}/\phi \approx \sqrt{G_{xy}/E_{yy}}$. Again, this discrepancy would be less for the polymer-matrix composite than the metal-matrix composite and should die out in both cases as E_{yy} is increased. However, in the case where θ is near the origin, (i.e. $\theta \leqslant \theta_{\varepsilon,\phi}$), where τ_{xy} rapidly fluctuates, the range over which τ_{xy} changes sign decreases, but fails to die out as $\varepsilon \to 0$. This is suggested by (29b) and (29e). Figure 15 shows a normalized plot for the same set of values for E_{yy} and $\sqrt{G_{xy}/E_{yy}}$ for the polymer-matrix composite for $N = 301$ and for matrix bay 4 or for $r/c = 0.0288$ when $\xi_c = 0$. Clearly, as E_{yy} increases, the shear oscillations do not appear in the crack tip region, and are in fact delayed until r reaches matrix bay $n \geqslant 10$. This effect was observed previously and is related to the elimination of the "dip" in the LEFM tensile stress profile of fibers $s = 2, 3, \ldots$. However, the LEFM τ_{xy} and the shear-lag τ_{xy} achieve good agreement as a result of an increased transverse stiffness E_{yy}. For a metal-matrix composite, similar behavior occurs, but for values of about $\varepsilon = E_{xx}/E_{yy}$ which must be about 2–8 times smaller.

Figures 16 and 17 compare the shear stresses at a point corresponding to the far right edge of matrix bay $s-1$ evaluated at a distance $r_s = [s-1+\Phi]w^*$ (see eqn (33)) from the crack tip predicted from LEFM with $E_{yy} = 10^8$ and from the shear-lag analysis. Clearly, the LEFM τ_{xy} peak stress is about half that of the shear lag τ_{xy}. We expect that the LEFM shear stress would be lower since it is evaluated at the far right edge of a matrix bay, which in the continuum version carries tension thereby leading to a reduced shear stress at the right edge. This suggests that we could improve shear stress agreement simply by choosing

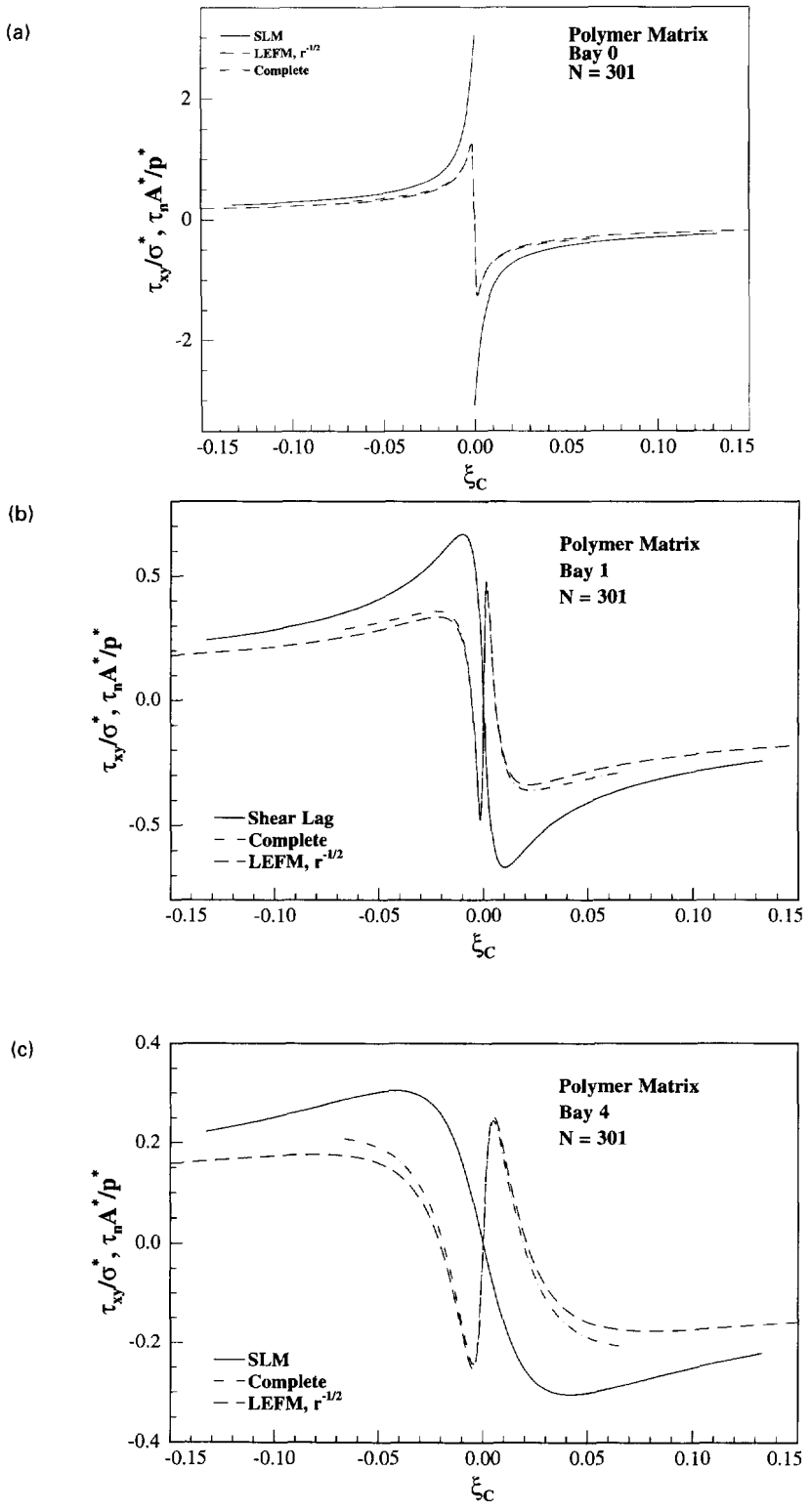

Fig. 13. Shear stress concentrations vs ξ_c (a) in the matrix region to the left of the first intact fiber, bay 0, (b) in bay 1 and (c) in bay 4, in a polymer-matrix composite predicted from the shear-lag analysis, LEFM, and the complete solution.

a point closer to the crack tip but in the corresponding matrix bay. For instance, recalculating using $\Phi/9$ in place of Φ in r_s of eqn (33) would provide the three-fold increase in the peak shear stress required for agreement in Figs 13(a) and (16). We, however, elect to remain consistent with previous shear stress calculations, but agreement improves rapidly

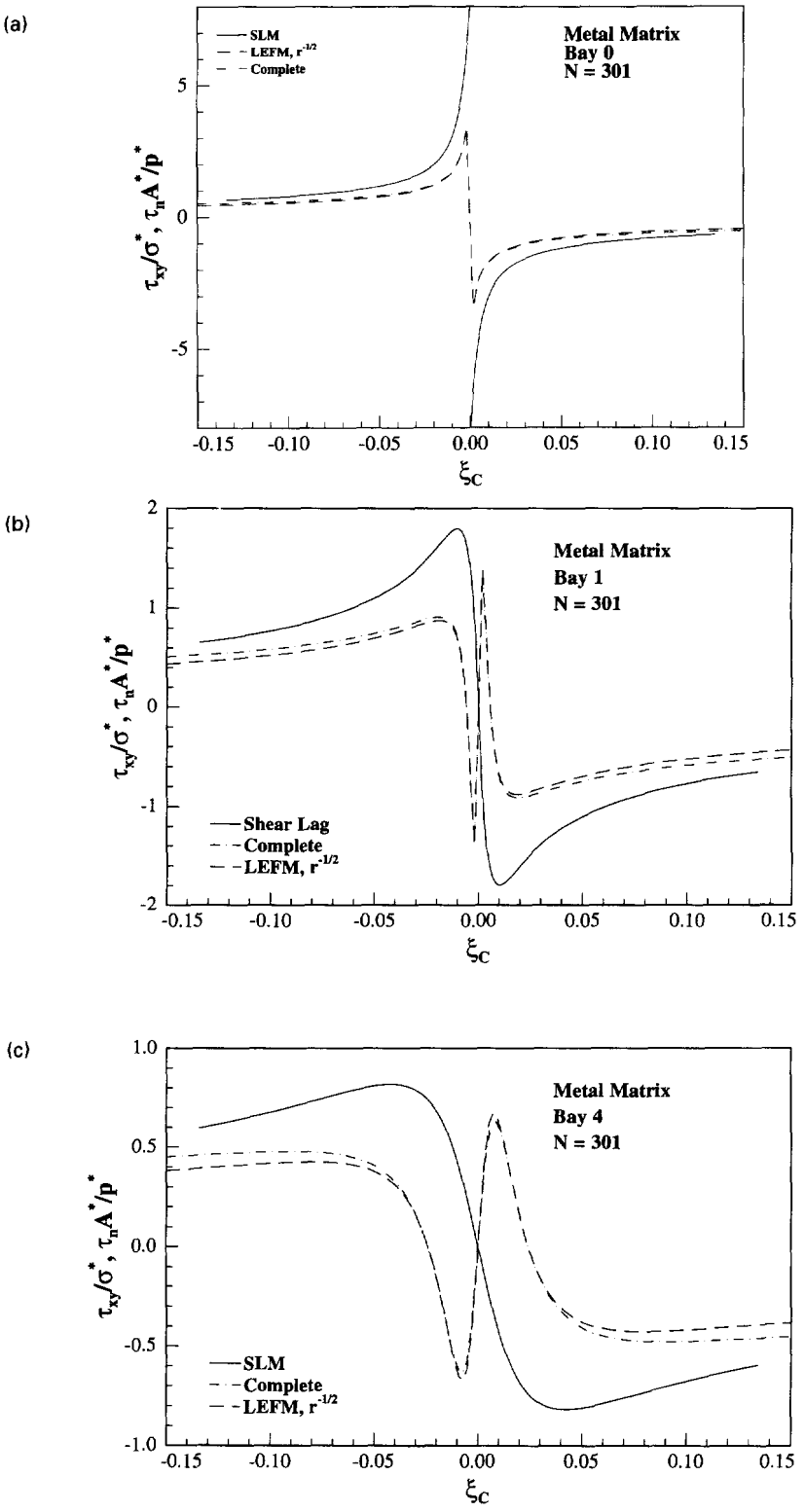

Fig. 14. Shear stress concentrations vs ξ_c (a) in the matrix region to the left of the first intact fiber, bay 0, (b) in bay 1, and (c) in bay 4, in a metal-matrix composite predicted from the shear-lag analysis, LEFM, and the complete solution.

by bay 4 (Fig. 17(b)). Figure 18 shows the same results for bays 0, 2 and 4 on a log-log scale natural to observing $1/\sqrt{r}$ behavior. Again, although the shear stresses from the LEFM solution are shifted downwards because of the chosen location of calculation, the two solutions have similar longitudinal decay behavior.

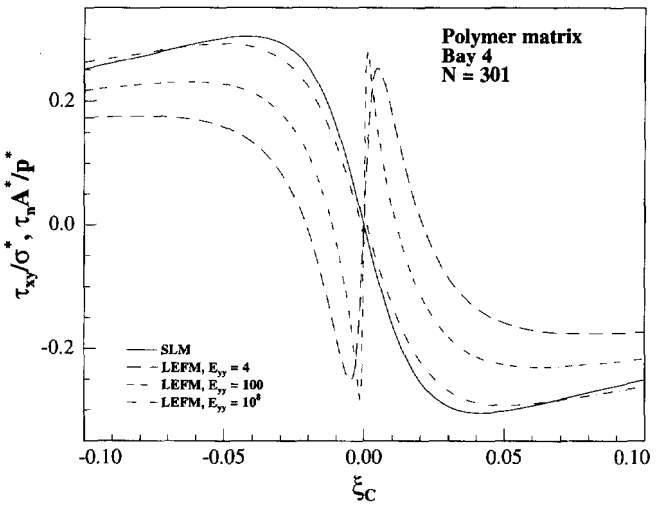

Fig. 15. Shear stress concentrations vs ξ_c in bay 4 in a polymer-matrix composite predicted from LEFM using various values of E_{yy} and the shear-lag analysis.

Since we are comparing results from linear elastic models, we expect unrealistically high predictions for the tensile and shear stress concentrations at the crack tip. From the extremely high shear stress concentrations found in Figs 13(a) and 14(a) for both composite types, it is reasonable to assume that interfacial debonding and plastic matrix yielding will most likely occur and consequently reduce the inner crack tip stress concentrations. Therefore, the corresponding tensile loads in the nearby fibers predicted from these linear elastic models are much higher than those which actually exist. For instance, from Figs 13(a) and 14(a), the maximum shear stress concentration in the matrix region surrounding the crack are 8.27 and 3.08 for the metal and polymer composite, respectively. If we assume typical values for the shear yield stress τ_y, $\tau_y = 50$ MPa for the polymer matrix and $\tau_y = 200$ MPa for the metal matrix, then the corresponding applied tensile loads to initiate yielding at the crack tip are $p^*/(w^*h) = 16.23$ MPa and $p^*/(w^*h) = 24.18$ MPa, respectively. Then from Figs 6(a) and 7(a), we find that the corresponding maximum tensile loads in the first intact fiber are 1213 MPa for the polymer matrix and 1806 MPa for the metal matrix. These values are much lower than the fiber strength for this length scale which is more like 5–10 GPa or higher. This means that edge stresses σ^* large enough to break fibers at the crack tip will cause massive matrix yielding and debonding.

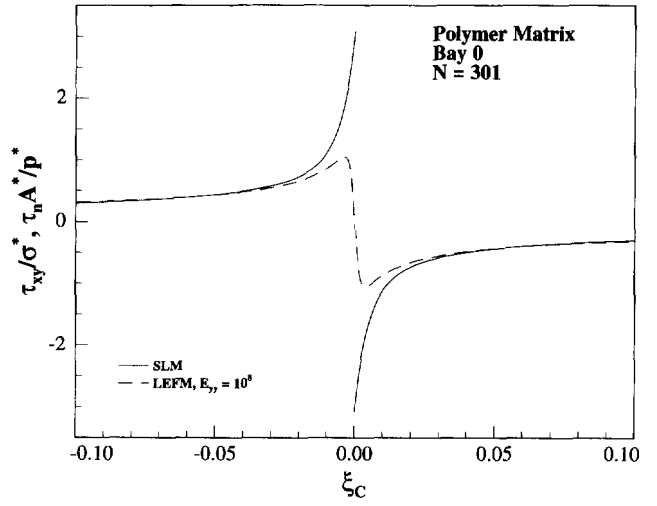

Fig. 16. Shear stress concentrations vs ξ_c in bay 0 in a polymer-matrix composite predicted from LEFM with $E_{yy} = 10^8$ and the shear-lag analysis.

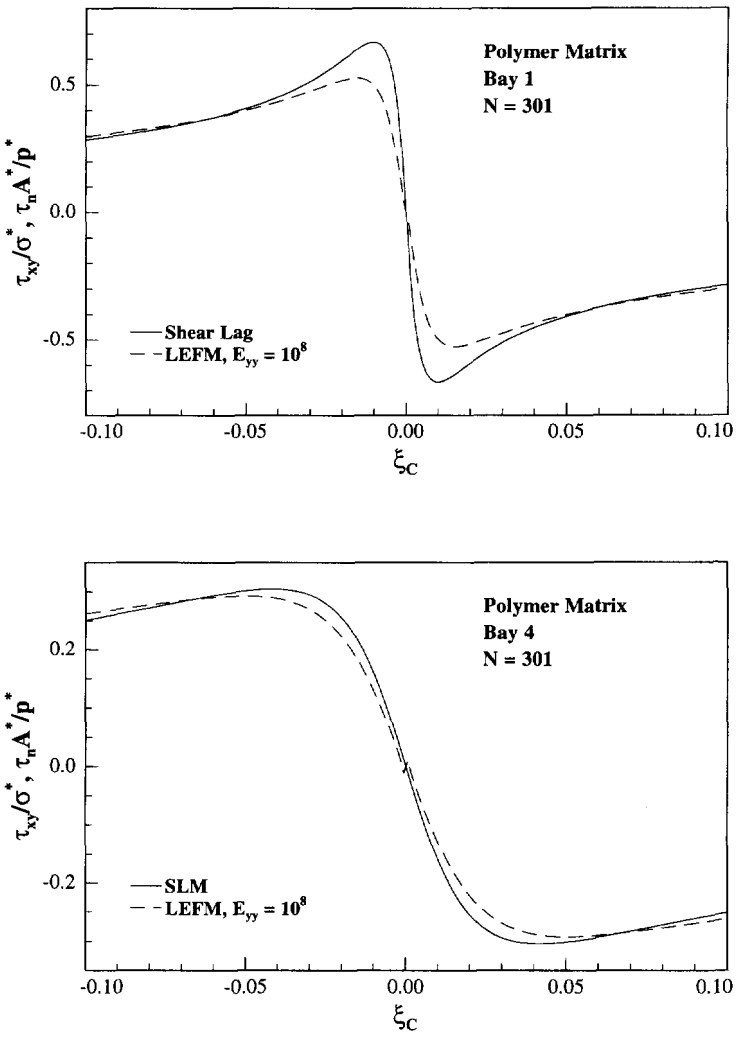

Fig. 17. Shear stress concentrations vs ξ_c in bay 1 and in bay 4, in a polymer-matrix composite predicted from LEFM with $E_{yy} = 10^8$ and the shear-lag analysis.

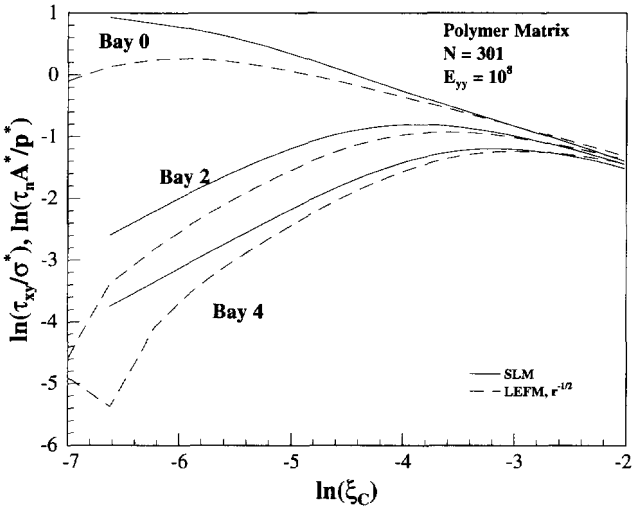

Fig. 18. Log-log plot of the shear stress concentrations vs ξ_c in bay 0, bay 2, and bay 4 in a polymer-matrix composite predicted from LEFM with $E_{yy} = 10^8$ and the shear-lag analysis.

Transverse tensile stresses

Next we compare the transverse tensile stresses, σ_{yy}, for a crack of length $2c = 2c_N$ with $N = 301$ and for the first intact fiber, r_s where $s = 1$. Results are given for the $1/\sqrt{r}$ LEFM solution only, since the shear-lag model does not generate these stresses, and therefore, the x coordinate is normalized to $\xi_c = x/(c\phi')$. Figure 19 plots the transverse tensile stress concentrations perpendicular to the fiber direction for the polymer matrix composite. In Fig. 19, E_{yy} is varied from 4 to 1×10^5 or $\varepsilon = E_{xx}/E_{yy}$ is varied from 12.5 to 5×10^{-4}. Clearly, these stresses resemble a narrow spike at $\xi_c = 0$ which increases with E_{yy}. Equations (29f)

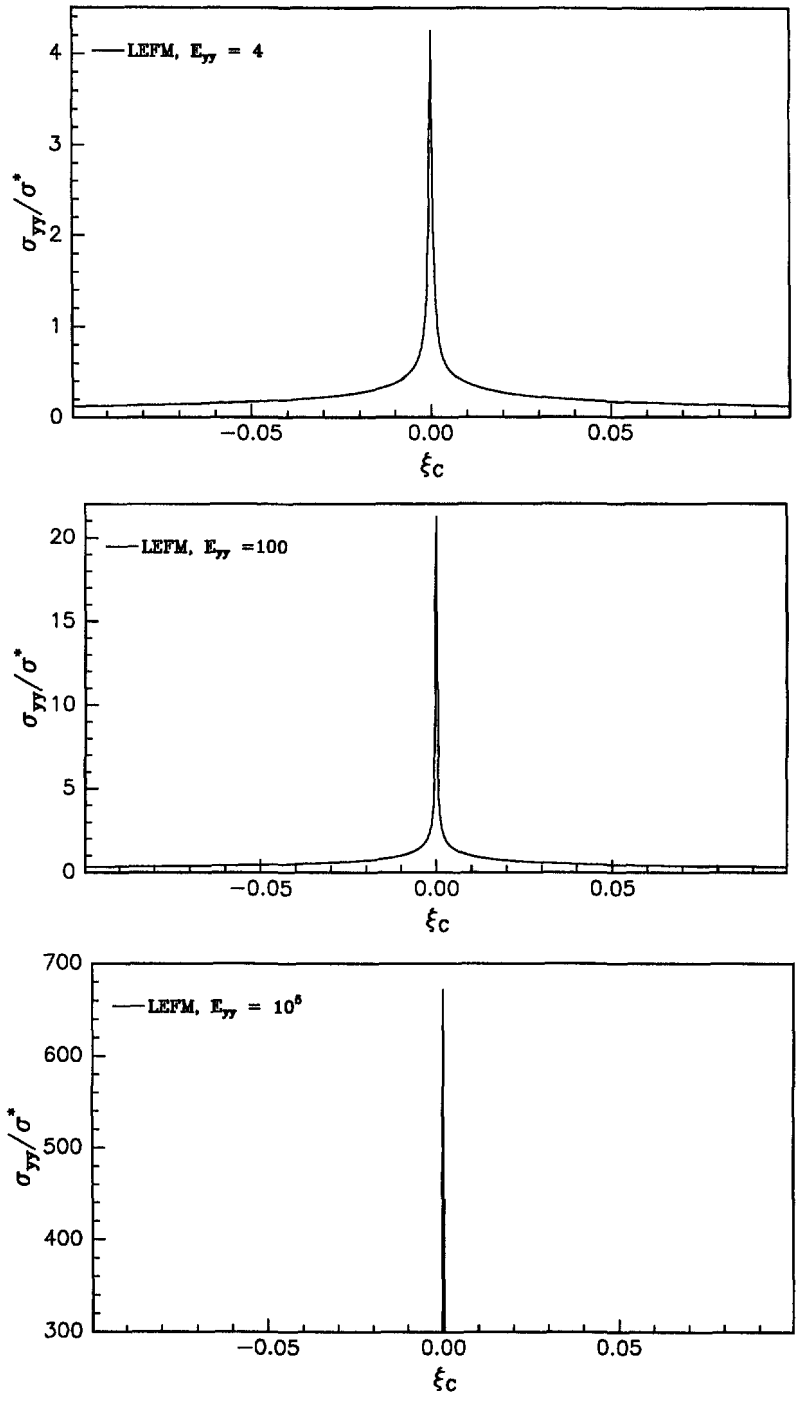

Fig. 19. Transverse tensile stress concentrations along the first fiber in a polymer-matrix composite predicted from LEFM using various values of E_{yy}.

Table 4: Behavior of transverse tensile stress σ_y in polymer matrix setting as E_{yy} and distance ahead of the "crack" is increased

$(E_{yy})_{polymer}$	Transverse stresses, σ_y/σ^* 4.0	100	1×10^5	1×10^8
Case 1. $s = 1$ $r/c_N = 0.0022$				
eqn (29f) $\theta = 0$	4.252	21.260	672.30	2.13×10^4
eqn (24b) $\theta = 0$	4.253	21.262	672.31	2.13×10^4
Case 2. $s = 1$ $r/c_N = 0.0022$				
eqn (29g) $\theta = \pi/2$	0.3674	0.9679	6.1734	35.5652
eqn (24b) $\theta \approx \pi/2$	0.1225	0.3222	2.0572	11.8548
Case 3. $s = 3$ $r/c_N = 0.0155$				
eqn (29g) $\theta = \pi/2$	0.1911	0.4273	2.4032	13.5142
eqn (24b) $\theta \approx \pi/2$	0.1202	0.3192	2.0538	11.8512
Case 4. $s = 6$ $r/c_N = 0.123$				
eqn (29g) $\theta = \pi/2$	0.0918	0.2419	1.5434	8.8915
eqn (24b) $\theta \approx \pi/2$	0.1188	0.3168	2.0505	11.8478

and (29g) suggest how these stresses should increase with ε and ϕ. Table 4 compares the asymptotic approximations (29f) and (29g) with the σ_{yy}/σ^* stress field eqn (24b) for $\theta = 0$ and $\theta = \pi/2$, respectively, and for $N = 301$. In this table, E_{yy} is varied from 4 to 10^8 with E_{xx} and G_{xy} fixed at 50 and 2, respectively, and for $s = 1$, 3, and 6 or for $0.002 < r/c < 0.03$ ahead of the crack traveling along the fiber. As shown in Table 4, the predictions of (29f) and (29g) work well. A main point is that these stresses are generally much larger than the matrix can sustain elastically.

6. CONCLUSIONS

In this study, we have restricted our attention to a unidirectional composite lamina containing a few hundred fiber breaks aligned on the y-axis and under uniform tension. For this case, the stress calculations from the LEFM and BIS technique do achieve good agreement in the crack-tip region where LEFM is valid. Also, this study shows that agreement improves as $E_{xx}/E_{yy} \to 0$ or when the transverse stiffness greatly exceeds the longitudinal stiffness of the composite. Agreement between this shear-lag theory based analysis and LEFM for a center crack composite lamina, not only increases confidence in the shear-lag model and reinforces its validity, but it also emphasizes some advantages of the shear-lag model. The BIS analysis has the advantage of evaluating the key stress distributions everywhere in an inhomogeneous, unidirectional fiber composite given any number (from one to several thousand) and any configuration of fiber breaks. This shear-lag approach can analyze a discretized composite lamina on a microstructural level or at the length scale necessary to find the fiber loads and displacements due to only a few breaks. Recall that a unidirectional composite is inhomogeneous primarily due to the variability in fiber strength and therefore, agreement between the shear-lag model and the LEFM solution for a crack containing only a few fiber breaks is not expected. On the other hand, unlike the shear-lag model as developed so far, LEFM also provides crack-tip stress solutions for Mode II and III cracks and under other combinations of loading.

In evaluating the fracture behavior of a fibrous composite, it is important that the analysis accurately predict the location, as well as the magnitude, of the maximum stress concentration. Since fiber strength varies along the fiber length, weaker fiber elements lying near the crack plane where the fiber is overstressed are most likely to break next. As an elastically deforming matrix can efficiently transmit load away from fiber breaks, the

overstressed region is approximately only a few fiber diameters. Thus, considering the likelihood of fiber failure anywhere in the overstressed region, fiber breaks may progress from fiber to fiber in a non-planar fashion until the composite reaches fracture instability. Experimental observations show that subsequent fiber breaks do indeed occur in the vicinity of the crack tip but not exactly in line with the crack (Awerbuch and Hahn, 1977; Jones and Goree, 1983). Clearly, if crack extension is non-planar then stress concentrations surrounding the fiber breaks are not as severe as those calculated assuming planar extension. Furthermore the energy required for crack propagation will be increased. The BIS technique can evaluate stresses surrounding any configuration of breaks and therefore, account for non-planar crack extension.

In many cases, the matrix in fibrous composites may exhibit plastic behavior leading possibly to a more ductile type fracture in the composite. In these composites, matrix yielding and debonding of the fiber-matrix interface occurs in regions around fiber breaks altering the matrix's load transmission capabilities. As a result, the stress distributions in the matrix and fibers are altered and less severe (Beyerlein *et al.*, 1995). In any case, it would be unrealistic to assume that the material behaves elastically in the region surrounding the crack tip. The two solutions compared in this study assume infinitely linear elastic behavior and, therefore, do not account for the inelastic behavior of the matrix. As a result, the crack-tip stress fields from both analyses contain unrealistically large values of fiber stress and matrix shear stress. Thus, these analyses would overestimate notch sensitivity or conservatively predict fracture strengths and so perhaps neither approach is valid for ductile matrix composites. However one suspects that when crack tip plasticity is introduced into the orthotropic LEFM theory and the results compared to shear-lag theory with an elastic-plastic matrix, so that large stresses are mitigated, the two theories will agree even better.

Considering this aspect further, recent exact analysis and accurate numerical calculations for one fiber break (modeled as a penny-shaped crack) in a three-dimensional composite have suggested that the shear-lag model gives unrealistic results for nearby fiber loads (Nedele and Wisnom, 1994; Case and Reifsnider, 1995). The difficulty with these linear elastic crack analyses, however, is that the matrix at the fiber break (or crack tip singularity) is predicted to have both axial tensile and shear stresses much higher than it can sustain in reality. In other words, if the unloaded fiber tensile stresses are not transmitted through shear to the adjacent fibers, they must be supported by the matrix at unrealistic magnitudes.

Models which account for plastic behavior before fracture and for non-planar crack extension better represent the fracture behavior of unidirectional fibrous composites. This is one reason why LEFM is inappropriate for predicting fracture in fiber reinforced metal-matrix composites and in any case, adding in plasticity for an orthotropic material is computationally a formidable task. On the other hand, the shear-lag model is a structurally based, simplified model which can potentially account for these various forms of damage. Previous work in extending the shear-lag model to account for plastic yielding achieves good agreement with experimental observations (Goree *et al.*, 1989). Also, other shear-lag based Monte-Carlo simulations and analytical models that incorporate matrix yielding and/or debonding find that the plastic yield zones are much larger than that of the theoretical plastic zone which surrounds the crack tip and relaxes the $1/\sqrt{r}$ stress singularity (Goree and Gross, 1979; Goree *et al.*, 1989; Rossettos and Olia, 1993; Tirosh, 1973).

Acknowledgements—The authors would like to thank A. Selvarathinam and J. G. Goree for providing results from their complete elasticity solution and for useful discussion. We also acknowledge the support of the AFOSR University Research Initiative (grant no. F49620-93-1-0235). This material is based upon work supported under a National Science Foundation Graduate Research Fellowship, and an NSF/GEE fellowship.

REFERENCES

Awerbuch, J. and Hahn, H. T. (1977). Fracture behavior of metal matrix composites. In *Proc. Soc. Engng Sci., Recent Advances in Engng Sci.*, Vol. 4, pp. 343–350.

Beyerlein, I. J., Phoenix, S. L., and Sastry, A. M. (1995). Stress concentrations around aligned fiber breaks in a unidirectional composite with an elastic-plastic matrix. In *Simulation of Materials Processing: Theory, Methods,*

and Applications, *NUMIFORM* 95 (eds Shen and Dawson). AA Balkema Publishers, Netherlands, pp. 237–242.

Case, S. W. and Reifsnider, K. L. (1995). Micromechanical analysis of fiber fracture in unidirectional composite materials.

Chou, T. W. (1992). *Microstructural Design of Fiber Composites*. Cambridge University Press, New York.

Dharani, L. R., Jones, W. F., and Goree, J. G. (1983). Mathematical modeling of damage in unidirectional composites. *Engng Fract. Mech.* **17,** 555–573.

Fichter, W. B. (1969). Stress concentrations around broken filaments in a filament-stiffened sheet. *NASA TN D-5453*.

Fukuda, H. and Chou, T. W. (1981). An advanced shear-lag model applicable to discontinuous fiber composites. *J. Comp. Mater.* **15,** 79–91.

Goda, K. and Phoenix, S. L. (1994). Reliability approach to the tensile strength of unidirectional CFRP composites by Monte-Carlo simulation in a shear-lag model. *Comp. Sci. Tech.* **50,** 457–468.

Goree, J. G., Dharani, L. R., and Jones, W. F. (1989). Crack growth and fracture of continuous fiber metal matrix composites: Analysis and experiments. In *Metal Matrix Composites: Testing, Analysis, and Failure Modes*, ASTM STP 1032 (ed. W. S. Johnson). American Society for Testing and Materials, Philadelphia, pp. 251–269.

Goree, J. G. and Gross, R. S. (1979). Analysis of a unidirectional composite containing broken fibers and matrix damage. *Engng Fract. Mech.* **13,** 563–578.

Goree, J. G. and Gross, R. S. (1980). Stresses in a three-dimensional unidirectional composite containing broken fibers. *Engng Fract. Mech.* **13,** 395–405.

Hedgepeth, J. M. (1961). Stress concentrations in filamentary structures. NASA TN D-882.

Hedgepeth, J. M. and Van Dyke, P. (1967). Local stress concentrations in imperfect filamentary composite materials. *J. Comp. Mat.* **1,** 294–309.

Hikami, F. and Chou, T. W. (1990). Explicit crack problem solutions of unidirectional composites: elastic stress concentrations. *AIAA J.* **28,** 499–505.

Jones, W. F. and Goree, J. G. (1983). Fracture behavior of unidirectional boron/Al composite laminates. *Mech. Comp. Mat., ASME AMD.* **58,** 171–178.

Lekhnitskii, S. G. (1963). *Theory of Elasticity of an Anisotropic Body*. Holden-Day, San Francisco.

Nedele, M. R. and Wisnom, M. R. (1994). Three-dimensional finite element analysis of the stress concentration at a single fibre break. *Comp. Sci. Tech.* **51,** 517–524.

Ochiai, S., Schulte, K., and Peters, P. W. M. (1991). Strain concentration factors for fibers and matrix in unidirectional composites. *Comp. Sci. Tech.* **41,** 237–256.

Reedy, E. D. (1984). Fiber stresses in a crack monolayer: Comparison of shear-lag and 3-D finite element predictions. *J. Comp. Mat.* **18,** 595–607.

Ross, S. M. (1993). *Introduction to Probability Models*, 5th Edn. Academic Press, Inc., New York.

Rossettos, J. N. and Olia, M. (1993). Stress concentration and post matrix yield at fiber breaks in hybrid composites. In *Proc 13th Army Symp. Solid Mechanics*. Plymouth, MA, pp. 201–212.

Rossettos, J. N. and Shishesaz, M. (1987). Stress concentration in fiber composite sheets including matrix extension. *J. Appl. Mech.* **54,** 723–724.

Sastry, A. M. (1994). Calculation of stress concentrations in damaged composite solids for determining strength distributions. Ph. D. thesis, Mechanical Engineering, Cornell University.

Sastry, A. M. and Phoenix, S. L. (1993). Load redistribution near non-aligned fibre breaks in a two-dimensional unidirectional composite using break-influence superposition, *J. Mat. Sci. Lett.* **12,** 1596–1599.

Selvarathinam, A. S. (1995). A generalized linear elastic fracture mechanics model for advanced materials. Ph. D. thesis, Department of Mechanical Engineering, Clemson University.

Sih, G. C. (1981). *Cracks in Composite Materials*. Martinus Nijhoff Publishers, Boston.

Tirosh, J. (1973). The effect of plasticity and crack blunting on the stress distribution in orthotropic composite materials. *J. Appl. Mech.* **40,** 785–790.

Van Dyke, P. and Hedgepeth, J. M. (1969). Stress concentrations from single-filament failures in composite materials. *Textile Res. J.* **39,** 618–626.

Wolla, J. M. and Goree, J. G. (1987). Experimental evaluation of longitudinal splitting in unidirectional composites. *J. Comp. Mat.* **21,** 49–67.